Results in Physics 54 (2023) 107113

Contents lists available at ScienceDirect

Results in Physics

journal homepage: www.elsevier.com/locate/rinp

Obliquely propagating optical wave patterns to the (2 + 1)-dimensional chiral nonlinear Schrödinger equation in the absence and presence of Atangana derivative

K.M. Abdul Al Woadud [a,b,*], Dipankar Kumar [c,*], Aminur Rahman Khan [a]

[a] Department of Mathematics, Jahangirnagar University, Savar, Dhaka 1342, Bangladesh
[b] Department of Electrical & Electronic Engineering, Uttara University, Dhaka 1230, Bangladesh
[c] Department of Mathematics, Bangabandhu Sheikh Mujibur Rahman Science and Technology University, Gopalganj 8100, Bangladesh

ARTICLE INFO

Keywords:
Chiral Schrödinger equation
The unified method
Optical solutions
Wave obliqueness
Atangana derivative
Wave propagation

ABSTRACT

The study aims to explore obliquely propagating optical wave solutions to the (2 + 1)-dimensional chiral nonlinear Schrödinger (NLS) equation in both the absence and presence of the Atangana derivative. In order to convert the classical-order chiral nonlinear Schrödinger equation to an ordinary differential equation, a transformation associated with wave obliqueness is applied. Hereafter, the unified method is applied to the reduced equation. As outcomes, the dark, periodic singular with unequal wave length, periodic with equal wavelength, periodic, unsmooth periodic, singular periodic soliton solutions are received to the ordinary differential equation. Later, the acquired solutions are then put to the applied transformation associated with obliqueness. Moreover, the fractional-order chiral NLS equation is solved by using the spatiotemporal Atangana derivative with oblique wave transformation and the unified method. In terms of wave obliqueness, fractionality, and applied technique sense, all generated wave solutions are revealed to be novel. Along with their physical explanations, the impacts of obliqueness and fractionality on the solutions are graphically illustrated. It is exposed that as obliqueness and fractionality increase, the optical wave phenomena change. Additionally, it is discovered that the employed method can be used to obtain novel optical soliton features to the chiral nonlinear Schrödinger equation with or without fractional and obliqueness constraints. It can be assured that the utilized method is more powerful than the other methods. As a result, the method can be used in future research to explain the many physical phenomena that arise in optical fiber communication networks.

Introduction

Background and motivation

Nonlinear partial differential equations (PDEs) govern a wide range of complex phenomena in the biological, chemical, and physical sciences. Many scientists working in this area are drawn to the well-known nonlinear Schrödinger equation because it makes it easier to understand complex phenomena that arise in fields like quantum physics, fluid dynamics, optical physics, and others. Due to the development of computational facilities, there have been tremendous breakthroughs in recent years in the resolving of the nonlinear PDEs by some important analytical methods, such as the homogeneous balance method [1], the extended F-expansion method [2], the extended tanh function method [3], the modified simple equation method [4], the (G'/G)-expansion method [5], the transformed rational function method [6], the generalized Kudryashov method [7], the auxiliary equation method [8], the Weierstrass elliptic function expansion method [9], the modified Kudryashov method [10–13], the sine-Gordon equation expansion method [14,15], the extended sinh-Gordon equation method [16–18], the hyperbolic function method [19], the Hirota method [20], the Sardar subequation method [21–23], the unified solver method [24]. Remarkably, three of the papers of Kudryashov [25–27] advise us to be careful when using the methods for obtaining exact solutions of the nonlinear PDEs. In this regard, we have checked our newly explored solutions under the back substitution of the correspondent PDE by Maple 18 software and found them correct.

* Corresponding authors.
E-mail addresses: woadudru50@gmail.com (K.M. Abdul Al Woadud), dks.bsmrstu@gmail.com (D. Kumar), aminur@juniv.edu (A. Rahman Khan).

https://doi.org/10.1016/j.rinp.2023.107113
Received 13 September 2023; Received in revised form 20 October 2023; Accepted 23 October 2023
Available online 30 October 2023

Governing model and literature review

Under the investigation of novel optical wave solutions, we consider the chiral NLS equation given by [28–31]:

$$i\psi_t + a(\psi_{xx} + \psi_{yy}) + i(b_1(\psi\psi_x^* - \psi^*\psi_x) + b_2(\psi\psi_y^* - \psi^*\psi_y))\psi = 0 \quad (1)$$

where $\psi = \psi(x, y, t)$ is the complex function of x, y and t. The spatial variables x and y and the temporal variable t are represented in Eq. (1). Eq. (1) denotes the temporal evolution of the wave, followed by the dispersion term that is given by the coefficient of a, b_1 and b_2 are nonlinear coupling constants and the '*' sign indicates the complex conjugate.

Equation (1) produces chiral solitons, which are crucial in the quantum Hall effect [28], where chirp and chiral excitations are known to manifest. Several studies have been conducted on the models (1). For example, Bulut et al., [29] contributed to solving the CNS equation and designed two types of progressing wave solutions such as bright and dark soliton trains. Moreover, Bulut et al., [29] identified bright and dark soliton solutions of the CNS equation with the aid of the extended sinh-Gordon equation method. Younis et al., [30] investigated the CNS equation critically with perturbation terms and a coefficient of Bohm potential. Consequently, by applying the extended tanh method along with their constraint conditions, soliton-like solutions, triangular-type solutions, and single and combined non-degenerate Jacobi elliptic function-like solutions can be derived. A trial solution technique is used for CNS equations [31]. The trial solution technique produces soliton and singular soliton solutions. Raza and Javid [29] conducted the optical dark and singular solitons for CNS equation by integrating two distinct integration schemes namely, the extended direct algebraic and extended trial equation methods. Based on the above literature [32–39], no studies have been found to construct analytic solutions for the (2 + 1)-dimensional chiral NLS equation with/without considering the Atangana's derivative and wave obliqueness. It is mentioned that some scholars used the unified method previously for solving a variety of types of nonlinear PDEs without or with the involvement of fractional calculus. However, most of them do not include wave obliqueness, as well as they are not explained from the physical point of view. Therefore, the present study will apply the unified method to the considered equation and interpret the spatiotemporal dynamics of soliton pulses in the absence and presence of the Atangana derivative combined with wave obliqueness.

Objectives of the study

The main objective of this study is

(i) to apply the unified method to interpret the spatiotemporal dynamics of optical soliton pulses in the (2 + 1)-D chiral NLS model with the absence and presence of the Atangana derivative,

(ii) to analyze the effects of wave obliqueness on the optical soliton pulses,

(iii) to interpret the effects of fractional parameters on the optical soliton pulses, and

(iv) to analyze the effects of free parameters related to the model and method on the optical soliton pulses, as well as, to interpret the method used for generating these pulses,

Recently, the unified method has attracted wide attention as it has huge potential in extracting new oblique optical wave solutions of the nonlinear PDEs with the absence and presence of fractional derivatives.

Methodology

In this section, we will recount the workflow of the unified method to investigate some new optical solutions to a nonlinear evolution equation (NLEE). Furthermore, the novelty of the unified method is discussed here.

Outlines of the unified method

Undertake a general (2 + 1)-dimensional NLEE in the following form:

$$P(\psi, \psi_x, \psi_y, \psi_t, \psi\psi_x, \psi_{xx}, \psi_{xy}, \psi_{xt}, \psi_{yt}, \psi\psi_{tt}, \psi_{xtt}, \cdots\cdots) = 0 \quad (2)$$

P is a polynomial of $\psi(x, y, t)$ and its various partial derivatives, which appear in both linear and nonlinear terms, where $\psi = \psi(x, y, t)$ is an unknown complex-valued function.

Step 1: With the introduction of the transformation

$$\psi(x, y, t) = u(\xi)e^{i\theta(x,y,t)} \quad (3)$$

where $\xi = \alpha cos\gamma x + \beta sin\gamma y - vt$ and $\theta(x, y, t) = pcos\gamma x + qsin\gamma y + wt$. Here, α and β denote the soliton's frequencies in the x- and y-directions, respectively, while w stands for the wave number. The soliton's inverse width in the x and y directions is represented by the parameters p and q, respectively, and its velocity is denoted by v. On the other hand, γ represents the obliqueness and is followed by the equation $cos^2\gamma + sin^2\gamma = 1$.

Eq. (2) is transformed into the following nonlinear ordinary differential equation (ODE):

$$O(u, uu', u', u'' \cdots\cdots\cdots) = 0 \quad (4)$$

where the superscripts represent the ordinary derivatives with respect to ξ, O is a polynomial of u and its derivatives. If necessary, one integrates Eq. (4) as many times as possible and sets the constants of integration to be zero for simplicity.

Step 2: Suppose the solution of a nonlinear PDE can be expressed by an ansatz as follows:

$$u(\xi) = a_0 + \sum_{i=1}^{M} (a_i\phi^i + b_i\phi^{-i}) \quad (5)$$

where $\phi = \phi(\xi)$ satisfies the Riccati differential equation

$$\phi'(\xi) = \phi^2(\xi) + \sigma \quad (6)$$

where $\phi' = \frac{d\phi}{d\xi}$, and a_i, b_i, and σ are constants. The general solutions of Eq. (6) are as follows:

Family 1: When $\sigma < 0$, the solutions of Eq. (6) are

$$\phi(\xi) = \begin{cases} \dfrac{\sqrt{-(R^2+S^2)\sigma} - R\sqrt{-\sigma}\,cosh(2\sqrt{-\sigma}(\xi+E))}{R\sinh(2\sqrt{-\sigma}(\xi+E)) + S} \\ \dfrac{-\sqrt{-(R^2+S^2)\sigma} - R\sqrt{-\sigma}\,cosh(2\sqrt{-\sigma}(\xi+E))}{R\sinh(2\sqrt{-\sigma}(\xi+E)) + S} \\ \sqrt{-\sigma} - \dfrac{2R\sqrt{-\sigma}}{R + cosh(2\sqrt{-\sigma}(\xi+E)) - sinh(2\sqrt{-\sigma}(\xi+E))} \\ -\sqrt{-\sigma} + \dfrac{2R\sqrt{-\sigma}}{R + cosh(2\sqrt{-\sigma}(\xi+E)) + sinh(2\sqrt{-\sigma}(\xi+E))} \end{cases} \quad (7)$$

Family 2: When $\sigma > 0$, the solutions of Eq. (6) are

$$\phi(\xi) = \begin{cases} \dfrac{\sqrt{(R^2-S^2)\sigma} - R\sqrt{\sigma}\,cos(2\sqrt{\sigma}(\xi+E))}{R\sin(2\sqrt{\sigma}(\xi+E)) + S} \\ \dfrac{-\sqrt{(R^2-S^2)\sigma} - R\sqrt{\sigma}\,cos(2\sqrt{\sigma}(\xi+E))}{R\sin(2\sqrt{\sigma}(\xi+E)) + S} \\ i\sqrt{\sigma} - \dfrac{2Ri\sqrt{\sigma}}{R + cos(2\sqrt{\sigma}(\xi+E)) - isin(2\sqrt{\sigma}(\xi+E))} \\ -i\sqrt{\sigma} + \dfrac{2Ri\sqrt{\sigma}}{R + cos(2\sqrt{\sigma}(\xi+E)) + isin(2\sqrt{\sigma}(\xi+E))} \end{cases} \quad (8)$$

Family 3: When $\sigma = 0$, the solution of Eq. (6) is

$$\phi(\xi) = -\frac{1}{\xi + E} \tag{9}$$

where R, S, and E are three real arbitrary constants.

Step 3: The positive integer M can be accomplished by considering the homogeneous balance between the linear term of the highest order with the nonlinear term of the highest degree appearing in Eq. (4) as follows: If it is defined that the degree of $u(\xi)$ as $D[u(\xi)] = M$, then the degree of the other expressions is defined by $D\left[\frac{d^q u}{d\xi^q}\right] = M + q$, $D\left[u^r\left(\frac{d^q u}{d\xi^q}\right)^s\right] = Mr + s(q+M)$. Thus, the value of M in Eq. (5) is found.

Step 4: Substituting Eq. (5) and Eq. (6) into Eq. (4) and collecting all terms with the same degree of ϕ together, then setting each coefficient of the term with $\phi^i(-M \le i \le M)$ to zero, yield a set of algebraic equations for a_i, b_i, v, w and σ. Substituting a_i, b_i, v, w and σ into Eq. (5). Using the general solutions of Eq. (6) in Eq. (7), Eq. (8), and Eq. (9) the explicit solutions of Eq. (2) immediately depending on the value of σ can be obtained.

Novelty of the unified method

The study of nonlinear PDEs has been pursued in several fields, including physics, biology, and chemistry. Therefore, it is crucial for scientists to develop new techniques and determine several solutions for nonlinear PDEs. The solution of nonlinear PDEs can be accomplished in numerous ways. The tanh function methods and the (G'/G) -expansion methods families are the two that are most frequently employed. The advantages of the unified method, firstly compared to other methods, it generates a huge number of solutions. Namely, it gives not only the solutions of the other methods but also new exact solutions not obtained using other methods. Secondly, it unifies the merits of all the methods in one method without needing extra effort. Lastly, it has a simple algorithm to apply on the computer. Unlike the others, it reduces the process on the computer as much as sometimes even calculated by hand. As in refs. [40,41], the unified method is novel and efficient because it overcomes the weaknesses and deficiencies of the existing methods, such as (i) the tanh-function method [42], (ii) the extended tanh-function method [3], (iii) the modified extended tanh function method [43], (iv) the complex tanh-function method [44], (v) the G'/G-expansion method [45], (vi) the generalized G'/G-expansion method [46], and (vii) the $(G'/G, 1/G)$-expansion method [47,48].

Mathematical analysis

Wave transformation in the absence of the Atangana derivative

To determine optical wave solutions of Eq. (1), the following transformation is selected:

$$\psi(x,y,t) = u(\xi)e^{i\theta(x,y,t)}, i = \sqrt{-1} \tag{10}$$

where $u(\xi)$ represents the amplitude component with $\xi = \alpha cos\gamma x + \beta sin\gamma y - vt$ and the phase component $\theta(x,y,t)$ of the soliton is defined as $\theta(x,y,t) = pcos\gamma x + qsin\gamma y + wt$. Here, α and β denote the soliton's frequencies in the x- and y-directions, respectively, while w stands for the wave number. Additionally, in Eq. (10), the parameters p and q stand for the inverse widths of the soliton along the x and y directions, respectively, while v stands for the soliton's velocity. It is noted here that γ represents the wave obliqueness $(0 \le \gamma < \pi/2)$ and $(\pi/2 < \gamma \le \pi)$. The integer-order CNS equation specified by Eq. (1) after applying the aforementioned transformation and dividing the result into real and imaginary parts, the following pair of equations is achieved:

$$\left.\begin{array}{l} Re : T_1 u'' + T_2 u^3 - (T_3 + w)u = 0 \\ Im : v = 2a\left(\alpha p cos^2\gamma + \beta q sin^2\gamma\right) \end{array}\right\} \tag{11}$$

where $T_1 = a(\alpha^2 cos^2\gamma + \beta^2 sin^2\gamma)$, $T_2 = 2(pb_1 cos\gamma + qb_2 sin\gamma)$, $T_3 = a(p^2 cos^2\gamma + q^2 sin^2\gamma)$, and a prime represents the derivative with respect to ξ.

Optical wave patterns of the model without the presence of the Atangana derivative

Balancing the linear term (u'') with a nonlinear term (u^3) in Eq. (11), we find $M = 1$. Then, the solution of Eq. (11) takes the form

$$u(\xi) = A_0 + A_1(\varphi(\xi)) + B_1(\varphi(\xi))^{-1} \tag{12}$$

By substituting Eq. (12) along with its second derivative into Eq. (11) and equating the like powers of $\varphi(\xi)$, a system of equations is attained, which on solving yields the following solution sets:

Set 1: $A_0 = 0$, $A_1 = 0$, $B_1 = \pm\sqrt{-\frac{2T_1}{T_2}}\sigma$, and $w = 2T_1\sigma - T_3$.

Set 2: $A_0 = 0$, $A_1 = \pm\sqrt{-\frac{2T_1}{T_2}}$, $B_1 = 0$, and $w = 2T_1\sigma - T_3$.

Set 3: $A_0 = 0$, $A_1 = \pm\sqrt{-\frac{2T_1}{T_2}}$, $B_1 = \pm\sqrt{-\frac{2T_1}{T_2}}\sigma$, and $w = -(4T_1\sigma + T_3)$.

Set 4: $A_0 = 0$, $A_1 = \mp\sqrt{-\frac{2T_1}{T_2}}$, $B_1 = \pm\sqrt{-\frac{2T_1}{T_2}}\sigma$, and $w = (8T_1\sigma - T_3)$.

where $T_1 = a(\alpha^2 cos^2\gamma + \beta^2 sin^2\gamma)$, $T_2 = 2(pb_1 cos\gamma + qb_2 sin\gamma)$, and $T_3 = a(p^2 cos^2\gamma + q^2 sin^2\gamma)$.

Set 1 corresponds to the following optical wave solutions with the obliqueness of the considered model with the aid of Eqs. (7)-(10):

$$\psi_{1,2}(x,y,t) = \pm\sqrt{-\frac{2T_1}{T_2}}\sigma\left(\frac{\sqrt{-(R^2+S^2)\sigma} - R\sqrt{-\sigma}cosh(2\sqrt{-\sigma}(\xi+E))}{R\sinh(2\sqrt{-\sigma}(\xi+E)) + S}\right)^{-1} \times e^{i\theta(x,y,t)} \tag{13}$$

$$\psi_{3,4}(x,y,t) = \pm\sqrt{-\frac{2T_1}{T_2}}\sigma\left(\frac{-\sqrt{-(R^2+S^2)\sigma} - R\sqrt{-\sigma}cosh(2\sqrt{-\sigma}(\xi+E))}{R\sinh(2\sqrt{-\sigma}(\xi+E)) + S}\right)^{-1} \times e^{i\theta(x,y,t)} \tag{14}$$

$$\psi_{5,6}(x,y,t) = \pm\sqrt{-\frac{2T_1}{T_2}}\sigma\left(\sqrt{-\sigma} - \frac{2R\sqrt{-\sigma}}{R + cosh(2\sqrt{-\sigma}(\xi+E)) - sinh(2\sqrt{-\sigma}(\xi+E))}\right)^{-1} \times e^{i\theta(x,y,t)} \tag{15}$$

$$\psi_{7,8}(x,y,t) = \pm\sqrt{-\frac{2T_1}{T_2}}\sigma\left(-\sqrt{-\sigma} + \frac{2R\sqrt{-\sigma}}{R + cosh(2\sqrt{-\sigma}(\xi+E)) + sinh(2\sqrt{-\sigma}(\xi+E))}\right)^{-1} \times e^{i\theta(x,y,t)} \quad 16)$$

$$\psi_{9,10}(x,y,t) = \pm\sqrt{-\frac{2T_1}{T_2}\sigma}\left(\frac{\sqrt{\left(R^2-S^2\right)\sigma} - R\sqrt{\sigma}\,cos(2\sqrt{\sigma}\,(\xi+E)\,)}{R\sin(2\sqrt{\sigma}\,(\xi+E)\,)+S}\right)^{-1} \times e^{i\theta(x,y,t)} \tag{17}$$

$$\psi_{19,20}(x,y,t) = \pm\sqrt{-\frac{2T_1}{T_2}}\left(\frac{-\sqrt{-\left(R^2+S^2\right)\sigma} - R\sqrt{-\sigma}\,cosh(2\sqrt{-\sigma}(\xi+E))}{R\sinh(2\sqrt{-\sigma}(\xi+E))+S}\right) \times e^{i\theta(x,y,t)} \tag{22}$$

$$\psi_{21,22}(x,y,t) = \pm\sqrt{-\frac{2T_1}{T_2}}\left(\sqrt{-\sigma} - \frac{2R\sqrt{-\sigma}}{R+cosh(2\sqrt{-\sigma}\,(\xi+E)\,)-sinh(2\sqrt{-\sigma}\,(\xi+E)\,)}\right) \times e^{i\theta(x,y,t)} \tag{23}$$

$$\psi_{23,24}(x,y,t) = \pm\sqrt{-\frac{2T_1}{T_2}}\left(-\sqrt{-\sigma} + \frac{2R\sqrt{-\sigma}}{R+cosh(2\sqrt{-\sigma}\,(\xi+E)\,)+sinh(2\sqrt{-\sigma}\,(\xi+E)\,)}\right) \times e^{i\theta(x,y,t)} \tag{24}$$

$$\psi_{11,12}(x,y,t) = \pm\sqrt{-\frac{2T_1}{T_2}\sigma}\left(\frac{-\sqrt{\left(R^2-S^2\right)\sigma} - R\sqrt{\sigma}\,cos(2\sqrt{\sigma}\,(\xi+E)\,)}{R\sin(2\sqrt{\sigma}\,(\xi+E)\,)+S}\right)^{-1} \times e^{i\theta(x,y,t)} \tag{18}$$

$$\psi_{13,14}(x,y,t) = \pm\sqrt{-\frac{2T_1}{T_2}\sigma}\left(i\sqrt{\sigma} - \frac{2Ri\sqrt{\sigma}}{R+cos(2\sqrt{\sigma}(\xi+E))-isin(2\sqrt{\sigma}(\xi+E))}\right)^{-1} \times e^{i\theta(x,y,t)} \tag{19}$$

$$\psi_{25,26}(x,y,t) = \pm\sqrt{-\frac{2T_1}{T_2}}\left(\frac{\sqrt{\left(R^2-S^2\right)\sigma} - R\sqrt{\sigma}\,cos(2\sqrt{\sigma}(\xi+E))}{R\sin(2\sqrt{\sigma}(\xi+E))+S}\right) \times e^{i\theta(x,y,t)} \tag{25}$$

$$\psi_{27,28}(x,y,t) = \pm\sqrt{-\frac{2T_1}{T_2}}\left(\frac{-\sqrt{\left(R^2-S^2\right)\sigma} - R\sqrt{\sigma}\,cos(2\sqrt{\sigma}(\xi+E))}{R\sin(2\sqrt{\sigma}(\xi+E))+S}\right) \times e^{i\theta(x,y,t)} \tag{26}$$

$$\psi_{29,30}(x,y,t) = \pm\sqrt{-\frac{2T_1}{T_2}}\left(i\sqrt{\sigma} - \frac{2Ri\sqrt{\sigma}}{R+cos(2\sqrt{\sigma}(\xi+E))-isin(2\sqrt{\sigma}(\xi+E))}\right) \times e^{i\theta(x,y,t)} \tag{27}$$

$$\psi_{15,16}(x,y,t) = \pm\sqrt{-\frac{2T_1}{T_2}\sigma}\left(-i\sqrt{\sigma} + \frac{2Ri\sqrt{\sigma}}{R+cos(2\sqrt{\sigma}\,(\xi+E)\,)+isin(2\sqrt{\sigma}\,(\xi+E)\,)}\right)^{-1} \times e^{i\theta(x,y,t)} \tag{20}$$

For Eqs. (13)-(20), $\xi = \alpha cos\gamma x + \beta sin\gamma y - \left(2a\left(\alpha pcos^2\gamma + \beta qsin^2\gamma\right)\right)t$, $\theta(x,y,t) = pcos\gamma x + qsin\gamma y + (2T_1\sigma - T_3)t$, $T_1 = a\left(\alpha^2cos^2\gamma + \beta^2sin^2\gamma\right)$, $T_2 = 2(pb_1cos\gamma + qb_2sin\gamma)$, and $T_3 = a\left(p^2cos^2\gamma + q^2sin^2\gamma\right)$ are used for the obtained solutions.

Set 2 corresponds to the following optical wave solutions with the obliqueness of the considered model with the aid of Eqs. (7)-(10):

$$\psi_{17,18}(x,y,t) = \pm\sqrt{-\frac{2T_1}{T_2}}\left(\frac{\sqrt{-\left(R^2+S^2\right)\sigma} - R\sqrt{-\sigma}\,cosh(2\sqrt{-\sigma}\,(\xi+E)\,)}{R\sinh(2\sqrt{-\sigma}\,(\xi+E)\,)+S}\right) \times e^{i\theta(x,y,t)} \tag{21}$$

$$\psi_{31,32}(x,y,t) = \pm\sqrt{-\frac{2T_1}{T_2}}\left(-i\sqrt{\sigma} + \frac{2Ri\sqrt{\sigma}}{R+cos(2\sqrt{\sigma}(\xi+E))+isin(2\sqrt{\sigma}(\xi+E))}\right) \times e^{i\theta(x,y,t)} \tag{28}$$

For Eqs. (21)-(28), $\xi = \alpha cos\gamma x + \beta sin\gamma y - \left(2a\left(\alpha pcos^2\gamma + \beta qsin^2\gamma\right)\right)t$, $\theta(x,y,t) = pcos\gamma x + qsin\gamma y + (2T_1\sigma - T_3)t$, $T_1 = a\left(\alpha^2cos^2\gamma + \beta^2sin^2\gamma\right)$, $T_2 = 2(pb_1cos\gamma + qb_2sin\gamma)$, and $T_3 = a\left(p^2cos^2\gamma + q^2sin^2\gamma\right)$ are used for the obtained solutions.

Set 3 corresponds to the following optical wave solutions with the obliqueness of the considered model with the aid of Eqs. (7)-(10):

$$\psi_{33,34}(x,y,t) = \pm\left(\sqrt{-\frac{2T_1}{T_2}}\left(\frac{\sqrt{-\left(R^2+S^2\right)\sigma} - R\sqrt{-\sigma}\,cosh(2\sqrt{-\sigma}\,(\xi+E)\,)}{R\sinh(2\sqrt{-\sigma}\,(\xi+E)\,)+S}\right) + \sqrt{-\frac{2T_1}{T_2}\sigma}\left(\frac{\sqrt{-\left(R^2+S^2\right)\sigma} - R\sqrt{-\sigma}\,cosh(2\sqrt{-\sigma}\,(\xi+E)\,)}{R\sinh(2\sqrt{-\sigma}\,(\xi+E)\,)+S}\right)^{-1}\right) \times e^{i\theta(x,y,t)} \tag{29}$$

$$\psi_{35,36}(x,y,t)=\pm\left(\sqrt{-\frac{2T_1}{T_2}}\left(\frac{-\sqrt{-\left(R^2+S^2\right)\sigma}-R\sqrt{-\sigma}cosh(2\sqrt{-\sigma}(\xi+E))}{R\sinh(2\sqrt{-\sigma}(\xi+E))+S}\right)+\sqrt{-\frac{2T_1}{T_2}}\sigma\left(\frac{-\sqrt{-\left(R^2+S^2\right)\sigma}-R\sqrt{-\sigma}cosh(2\sqrt{-\sigma}(\xi+E))}{R\sinh(2\sqrt{-\sigma}(\xi+E))+S}\right)^{-1}\right)\times e^{i\theta(x,y,t)} \tag{30}$$

$$\begin{aligned}\psi_{37,38}(x,y,t)=\pm&\left(\sqrt{-\frac{2T_1}{T_2}}\left(\sqrt{-\sigma}-\frac{2R\sqrt{-\sigma}}{R+cosh(2\sqrt{-\sigma}(\xi+E))-sinh(2\sqrt{-\sigma}(\xi+E))}\right)\right.\\&\left.+\sqrt{-\frac{2T_1}{T_2}}\sigma\left(\sqrt{-\sigma}-\frac{2R\sqrt{-\sigma}}{R+cosh(2\sqrt{-\sigma}(\xi+E))-sinh(2\sqrt{-\sigma}(\xi+E))}\right)^{-1}\right)\times e^{i\theta(x,y,t)}\end{aligned} \tag{31}$$

$$\begin{aligned}\psi_{39,40}(x,y,t)=\pm&\left(\sqrt{-\frac{2T_1}{T_2}}\left(-\sqrt{-\sigma}+\frac{2R\sqrt{-\sigma}}{R+cosh(2\sqrt{-\sigma}(\xi+E))+sinh(2\sqrt{-\sigma}(\xi+E))}\right)\right.\\&\left.+\sqrt{-\frac{2T_1}{T_2}}\sigma\left(-\sqrt{-\sigma}+\frac{2R\sqrt{-\sigma}}{R+cosh(2\sqrt{-\sigma}(\xi+E))+sinh(2\sqrt{-\sigma}(\xi+E))}\right)^{-1}\right)\times e^{i\theta(x,y,t)}\end{aligned} \tag{32}$$

$$\psi_{41,42}(x,y,t)=\pm\left(\sqrt{-\frac{2T_1}{T_2}}\left(\frac{\sqrt{\left(R^2-S^2\right)\sigma}-R\sqrt{\sigma}cos(2\sqrt{\sigma}(\xi+E))}{R\sin(2\sqrt{\sigma}(\xi+E))+S}\right)+\sqrt{-\frac{2T_1}{T_2}}\sigma\left(\frac{\sqrt{\left(R^2-S^2\right)\sigma}-R\sqrt{\sigma}cos(2\sqrt{\sigma}(\xi+E))}{R\sin(2\sqrt{\sigma}(\xi+E))+S}\right)^{-1}\right)\times e^{i\theta(x,y,t)} \tag{33}$$

$$\psi_{43,44}(x,y,t)=\pm\left(\sqrt{-\frac{2T_1}{T_2}}\left(\frac{-\sqrt{\left(R^2-S^2\right)\sigma}-R\sqrt{\sigma}cos(2\sqrt{\sigma}(\xi+E))}{R\sin(2\sqrt{\sigma}(\xi+E))+S}\right)+\sqrt{-\frac{2T_1}{T_2}}\sigma\left(\frac{-\sqrt{\left(R^2-S^2\right)\sigma}-R\sqrt{\sigma}cos(2\sqrt{\sigma}(\xi+E))}{R\sin(2\sqrt{\sigma}(\xi+E))+S}\right)^{-1}\right)\times e^{i\theta(x,y,t)} \tag{34}$$

$$\psi_{45,46}(x,y,t)=\pm\left(\sqrt{-\frac{2T_1}{T_2}}\left(i\sqrt{\sigma}-\frac{2Ri\sqrt{\sigma}}{R+cos(2\sqrt{\sigma}(\xi+E))-isin(2\sqrt{\sigma}(\xi+E))}\right)+\sqrt{-\frac{2T_1}{T_2}}\sigma\left(i\sqrt{\sigma}-\frac{2Ri\sqrt{\sigma}}{R+cos(2\sqrt{\sigma}(\xi+E))-isin(2\sqrt{\sigma}(\xi+E))}\right)^{-1}\right)\times e^{i\theta(x,y,t)} \tag{35}$$

$$\begin{aligned}\psi_{47,48}(x,y,t)=\pm&\left(\sqrt{-\frac{2T_1}{T_2}}\left(-i\sqrt{\sigma}+\frac{2Ri\sqrt{\sigma}}{R+cos(2\sqrt{\sigma}(\xi+E))+isin(2\sqrt{\sigma}(\xi+E))}\right)\right.\\&\left.+\sqrt{-\frac{2T_1}{T_2}}\sigma\left(-i\sqrt{\sigma}+\frac{2Ri\sqrt{\sigma}}{R+cos(2\sqrt{\sigma}(\xi+E))+isin(2\sqrt{\sigma}(\xi+E))}\right)^{-1}\right)\times e^{i\theta(x,y,t)}\end{aligned} \tag{36}$$

$$\psi_{49,50}(x,y,t)=\mp\left(\sqrt{-\frac{2T_1}{T_2}}\left(-\frac{1}{\xi+E}\right)+\sqrt{-\frac{2T_1}{T_2}}\sigma\left(-\frac{1}{\xi+E}\right)^{-1}\right)\times e^{i\theta(x,y,t)},\ \text{when}\ \sigma=0 \tag{37}$$

For Eqs. (29)-(37), $\xi = \alpha cos\gamma x + \beta sin\gamma y - \left(2a\left(\alpha p cos^2\gamma + \beta q sin^2\gamma\right)\right)t$, $\theta(x,y,t) = pcos\gamma x + qsin\gamma y - (4T_1\sigma + T_3)t$, $T_1 = a\left(\alpha^2cos^2\gamma + \beta^2 sin^2\gamma\right)$, $T_2 = 2(pb_1cos\gamma + qb_2sin\gamma)$, and $T_3 = a\left(p^2cos^2\gamma + q^2sin^2\gamma\right)$ are used for the obtained solutions.

Set 4 corresponds to the following optical wave solutions with the obliqueness of the considered model with the aid of Eqs. (7)-(10):

$$\psi_{51,52}(x,y,t)=\mp\left(\sqrt{-\frac{2T_1}{T_2}}\left(\frac{\sqrt{-\left(R^2+S^2\right)\sigma}-R\sqrt{-\sigma}cosh(2\sqrt{-\sigma}(\xi+E))}{R\sinh(2\sqrt{-\sigma}(\xi+E))+S}\right)-\sqrt{-\frac{2T_1}{T_2}}\sigma\left(\frac{\sqrt{-\left(R^2+S^2\right)\sigma}-R\sqrt{-\sigma}cosh(2\sqrt{-\sigma}(\xi+E))}{R\sinh(2\sqrt{-\sigma}(\xi+E))+S}\right)^{-1}\right)\times e^{i\theta(x,y,t)} \tag{38}$$

$$\psi_{53,54}(x,y,t)=\mp\left(\sqrt{-\frac{2T_1}{T_2}}\left(\frac{-\sqrt{-\left(R^2+S^2\right)\sigma}-R\sqrt{-\sigma}cosh(2\sqrt{-\sigma}(\xi+E))}{R\sinh(2\sqrt{-\sigma}(\xi+E))+S}\right)-\sqrt{-\frac{2T_1}{T_2}}\sigma\left(\frac{-\sqrt{-\left(R^2+S^2\right)\sigma}-R\sqrt{-\sigma}cosh(2\sqrt{-\sigma}(\xi+E))}{R\sinh(2\sqrt{-\sigma}(\xi+E))+S}\right)^{-1}\right)\times e^{i\theta(x,y,t)} \tag{39}$$

$$\psi_{55,56}(x,y,t) = \mp\left(\sqrt{-\frac{2T_1}{T_2}}\left(\sqrt{-\sigma} - \frac{2R\sqrt{-\sigma}}{R + cosh(2\sqrt{-\sigma}(\xi+E)) - sinh(2\sqrt{-\sigma}(\xi+E))}\right) - \sqrt{-\frac{2T_1}{T_2}}\sigma\left(\sqrt{-\sigma} - \frac{2R\sqrt{-\sigma}}{R + cosh(2\sqrt{-\sigma}(\xi+E)) - sinh(2\sqrt{-\sigma}(\xi+E))}\right)^{-1}\right) \times e^{i\theta(x,y,t)} \tag{40}$$

$$\psi_{57,58}(x,y,t) = \mp\left(\sqrt{-\frac{2T_1}{T_2}}\left(-\sqrt{-\sigma} + \frac{2R\sqrt{-\sigma}}{R + cosh(2\sqrt{-\sigma}(\xi+E)) + sinh(2\sqrt{-\sigma}(\xi+E))}\right) - \sqrt{-\frac{2T_1}{T_2}}\sigma\left(-\sqrt{-\sigma} + \frac{2R\sqrt{-\sigma}}{R + cosh(2\sqrt{-\sigma}(\xi+E)) + sinh(2\sqrt{-\sigma}(\xi+E))}\right)^{-1}\right) \times e^{i\theta(x,y,t)} \tag{41}$$

$$\psi_{59,60}(x,y,t) = \mp\left(\sqrt{-\frac{2T_1}{T_2}}\left(\frac{\sqrt{(R^2-S^2)\sigma} - R\sqrt{\sigma}cos(2\sqrt{\sigma}(\xi+E))}{R\sin(2\sqrt{\sigma}(\xi+E)) + S}\right) - \sqrt{-\frac{2T_1}{T_2}}\sigma\left(\frac{\sqrt{(R^2-S^2)\sigma} - R\sqrt{\sigma}cos(2\sqrt{\sigma}(\xi+E))}{R\sin(2\sqrt{\sigma}(\xi+E)) + S}\right)^{-1}\right) \times e^{i\theta(x,y,t)} \tag{42}$$

$$\psi_{61,62}(x,y,t) = \mp\left(\sqrt{-\frac{2T_1}{T_2}}\left(\frac{-\sqrt{(R^2-S^2)\sigma} - R\sqrt{\sigma}cos(2\sqrt{\sigma}(\xi+E))}{R\sin(2\sqrt{\sigma}(\xi+E)) + S}\right) - \sqrt{-\frac{2T_1}{T_2}}\sigma\left(\frac{-\sqrt{(R^2-S^2)\sigma} - R\sqrt{\sigma}cos(2\sqrt{\sigma}(\xi+E))}{R\sin(2\sqrt{\sigma}(\xi+E)) + S}\right)^{-1}\right) \times e^{i\theta(x,y,t)} \tag{43}$$

$$\psi_{63,64}(x,y,t) = \mp\left(\sqrt{-\frac{2T_1}{T_2}}\left(i\sqrt{\sigma} - \frac{2Ri\sqrt{\sigma}}{R+cos(2\sqrt{\sigma}(\xi+E)) - isin(2\sqrt{\sigma}(\xi+E))}\right) - \sqrt{-\frac{2T_1}{T_2}}\sigma\left(i\sqrt{\sigma} - \frac{2Ri\sqrt{\sigma}}{R+cos(2\sqrt{\sigma}(\xi+E)) - isin(2\sqrt{\sigma}(\xi+E))}\right)^{-1}\right) \times e^{i\theta(x,y,t)} \tag{44}$$

$$\psi_{65,66}(x,y,t) = \mp\left(\sqrt{-\frac{2T_1}{T_2}}\left(-i\sqrt{\sigma} + \frac{2Ri\sqrt{\sigma}}{R + cos(2\sqrt{\sigma}(\xi+E)) + isin(2\sqrt{\sigma}(\xi+E))}\right) - \sqrt{-\frac{2T_1}{T_2}}\sigma\left(-i\sqrt{\sigma} + \frac{2Ri\sqrt{\sigma}}{R + cos(2\sqrt{\sigma}(\xi+E)) + isin(2\sqrt{\sigma}(\xi+E))}\right)^{-1}\right) \times e^{i\theta(x,y,t)} \tag{45}$$

$$\psi_{67,68}(x,\ y,\ t) = \pm\left(\sqrt{-\frac{2T_1}{T_2}}\left(-\frac{1}{\xi+E}\right) - \sqrt{-\frac{2T_1}{T_2}}\sigma\left(-\frac{1}{\xi+E}\right)^{-1}\right) \times e^{i\theta(x,y,t)},\ \text{when}\ \sigma = 0 \tag{46}$$

For Eqs. (38)-(46), $\xi = \alpha cos\gamma x + \beta sin\gamma y - (2a(\alpha pcos^2\gamma + \beta qsin^2\gamma))t$, $\theta(x,y,t) = pcos\gamma x + qsin\gamma y + (8T_1\sigma - T_3)t$, $T_1 = a(\alpha^2cos^2\gamma + \beta^2sin^2\gamma)$, $T_2 = 2(pb_1cos\gamma + qb_2sin\gamma)$, and $T_3 = a(p^2cos^2\gamma + q^2sin^2\gamma)$ are used for the obtained solutions.

It is notable to mention here that the obtained hyperbolic function solutions and trigonometric function solutions are valid for $\sigma < 0$ and $\sigma > 0$, respectively.

Graphical explanations of the explored optical solutions

Mathematical forms of the constructed solutions of the chiral NLS equation represent dark, periodic-singular with unequal wavelength, periodic with equal wavelength, unsmooth periodic, and other solitons profiles. All of the exerted solutions, we only plotted graphically along with their physical descriptions of the obtained solutions, given by Eq. (13), Eq. (17), Eq. (21), Eq. (25), Eq. (27), Eq. (36), and Eq. (43), which represent dark, periodic-singular with unequal wavelength, dark, periodic with equal wavelength, periodic, unsmooth periodic, singular periodic and other soliton solutions, respectively.

To demonstrate the underlying behaviors of the governing model, the obtained solutions to the chiral NLS equation for specific values of the free parameters are provided as 3D and 2D graphical illustrations. Fig. 1**(a)–1(c)** display spatiotemporal 3D graphs for the real, imaginary, and modulus components of the optical solution $\psi_1(x,y=0,t)$, respectively. Every real and imaginary part of $\psi_1(x,y=0,t)$ describes a periodic soliton. On the other hand, a dark soliton is indicated by the modulus portion of the aforementioned solution (see Fig. 1**(c)**). The 2D cross-sectional line plots of these behaviors at $t = 0$, which are shown in Fig. 1**(d)–1(f),** respectively, can confirm the sorts of behaviors indicated below. The real, imaginary, and modulus parts of the optical soliton $\psi_9(x,y=0,t)$ are shown in Fig. 2**(a)–2(c)** as spatiotemporal fluctuations, whereas Fig. 2**(d)–2(f)** show, respectively, 2D line graphs of the real and imaginary components, as well as the modulus of the aforementioned solution at time $t = 0$. The real and imaginary parts of $\psi_9(x, y=0,t)$ demonstrate periodic singular with unequal wave length solitons, which are shown in Fig. 2**(a) and 2(b),** respectively, whereas $|\psi_9(x,y=0,t)|$ designates a periodic-singular with unequal wavelength soliton (see Fig. 2**(c)**). These singular soliton solutions are confirmed by their 2D plots at $t = 0$, which are illustrated in Fig. 2**(d)–2(f)**, respectively. The same characteristics have been found for the obtained solution $\psi_{17}(x,y=0,t)$ that of $\psi_1(x,y=0,t)$, which are displayed in Fig. 3 **(a)–3(f).** Moreover, Fig. 4**(a)–4(c)** display periodic soliton with equal wavelength for each of real, imaginary, and absolute parts of $\psi_{25}(x,y=0,t)$. These periodic soliton solutions are confirmed by their 2D plots at $t = 0$, which are illustrated in Fig. 4**(d)–4(f)**, respectively. The 3D plots for the real and imaginary parts of $\psi_{29}(x,y=0,t)$ are exposed in Fig. 5**(a) and 5(b)**, respectively, which indicate periodic solutions but unequal wavelength. However, $|\psi_{29}(x,y=0,t)|$ yields also a periodic soliton with equal wavelength (see Fig. 5**(c)**). The 2D cross-sectional line plot of real, imaginary, and modulus parts of $\psi_{29}(x,y=0, t)$ at $t = 0$ are demonstrated in Fig. 5**(d)–5(f),** respectively. In Fig. 6**(a) and 6(b)**, respectively, each of the 3D representations of the real and imaginary portion of $\psi_{47}(x,y=0,t)$ depicts an unsmooth periodic soliton. But the graphical illustration of $|\psi_{47}(x,y=0,t)|$ gives a smooth periodic soliton (see Fig. 6**(c)**). The shape of the smooth and unsmooth

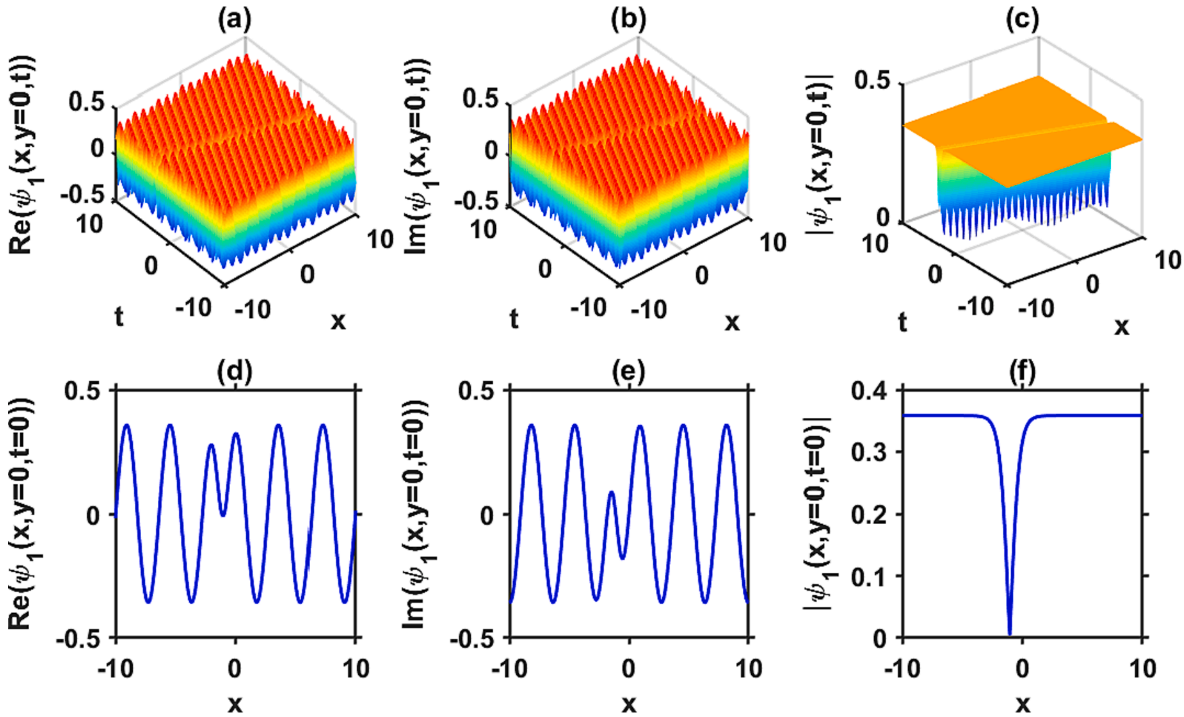

Fig. 1. Spatiotemporal illustrations of the obtained optical soliton solution given by Eq. (13) of (a) $\mathrm{Re}(\psi_1(x,y=0,t))$, (b) $Im(\psi_1(x,y=0,t))$, and (c) $|\psi_1(x,y=0,t)|$ under the selection of free parameters related to the model and method as $p=2, q=2, b_1=5, b_2=5, \alpha=1.5, \beta=-0.5, a=-1, \sigma=-1, R=-5, S=-5, E=1, \gamma=30^0$ in the xt-plane, and (d)-(f) 2D cross-sectional line plots of (a)-(c) at $t=0$, respectively.

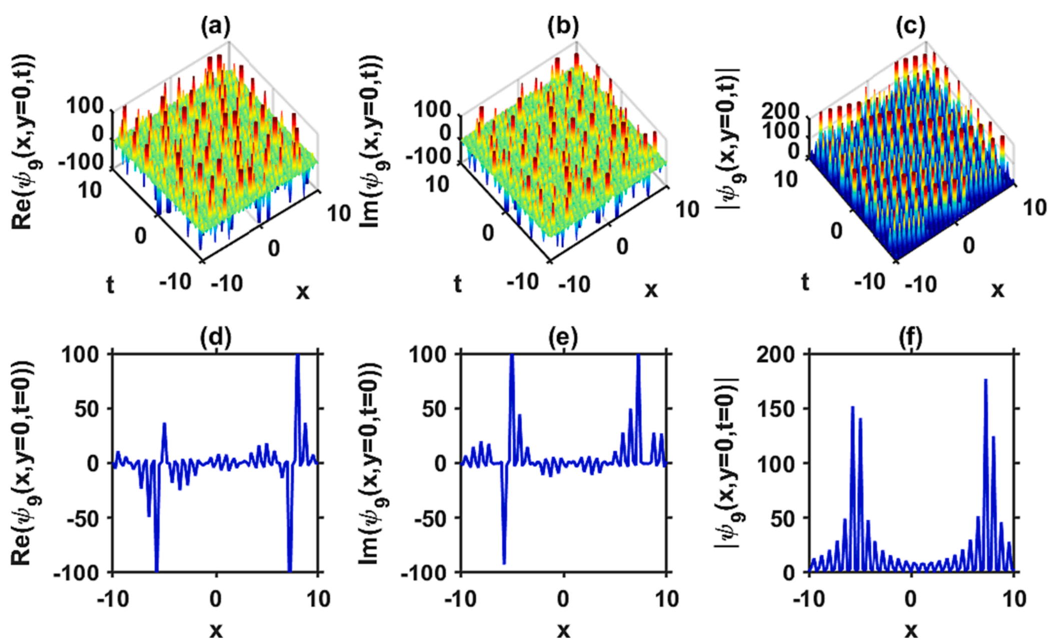

Fig. 2. Spatiotemporal illustrations of the obtained optical soliton solution given by Eq. (17) of (a) $\mathrm{Re}(\psi_9(x,y=0,t))$, (b) $Im(\psi_9(x,y=0,t))$, and (c) $|\psi_9(x,y=0,t)|$ under the selection of free parameters related to the model and method as $p=1, q=1, b_1=1, b_2=1, \alpha=1.5, \beta=2, a=-1, \sigma=10, R=1, S=1, E=0, \gamma=30^0$ in the xt-plane, and (d)-(f) 2D cross-sectional line plots of (a)-(c) at $t=0$, respectively.

periodic solitons is confirmed by their 2D plots (see Fig. 6**(d)–6(f)**). The real and imaginary parts of $\psi_{61}(x,y=0,t)$ demonstrate periodic-singular (see Fig. 7**(a)-(b)**), whereas $|\psi_{61}(x,y=0,t)|$ represent *U*-shaped periodic soliton (see Fig. 7**(c)**). The 2D plots of these periodic-singular soliton solutions at $t=0$, which are displayed in Fig. 7**(d)–7 (f),** respectively, corroborate the existence of these solutions.

Optical solitons of the CNS model in the presence of Atangana derivative

Preliminaries of fractional derivative

A generalization of classical calculus is fractional calculus. It has numerous uses in many different branches of mathematics, physics, and engineering. Fractional partial differential equations (FPDEs), which are

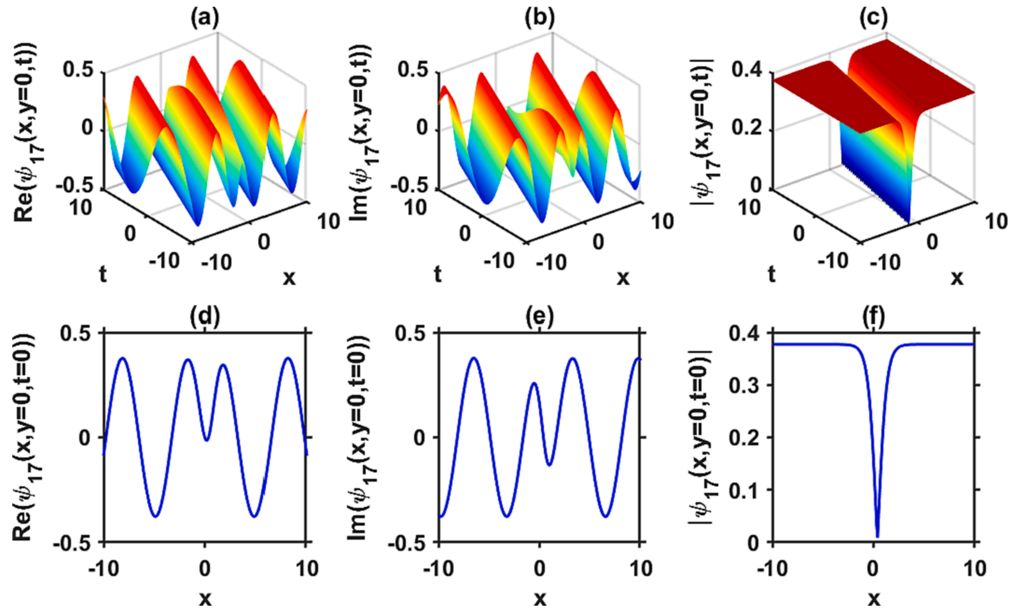

Fig. 3. Spatiotemporal illustrations of the obtained optical soliton solution given by Eq. (21) of (a) $\mathrm{Re}(\psi_{17}(x, y = 0, t))$, (b) $Im(\psi_{17}(x, y = 0, t))$, and (c) $|\psi_{17}(x, y = 0, t)|$ under the selection of free parameters related to the model and method as $p = 1, q = 1, b_1 = 1, b_2 = 0.1, \alpha = 1.2, \beta = -1, a = 0.1, \sigma = -1, R = 1, S = 1, E = 0, \gamma = 15^0$ in the xt-plane, and (d)-(f) 2D cross-sectional line plots of (a)-(c) at $t = 0$, respectively.

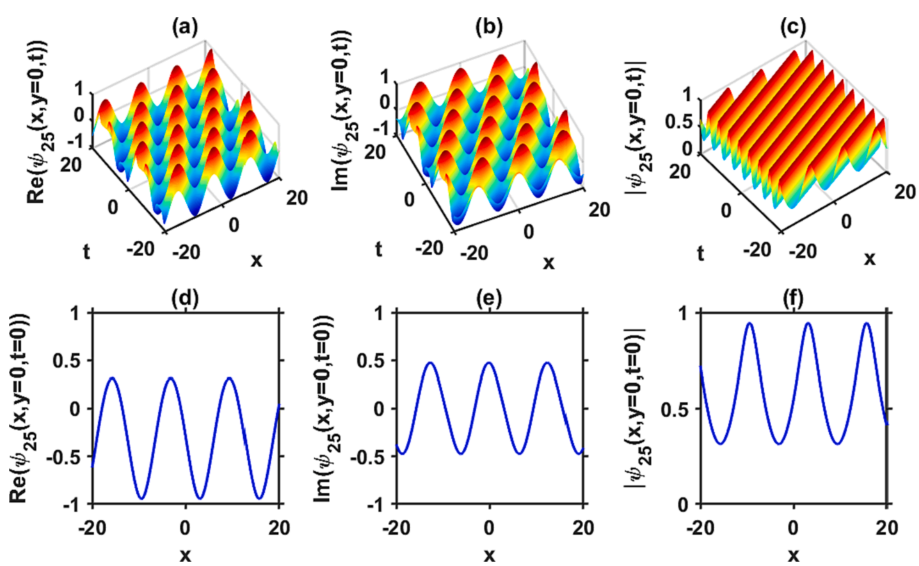

Fig. 4. Spatiotemporal illustrations of the obtained optical soliton solution given by Eq. (25) of (a) $\mathrm{Re}(\psi_{25}(x, y = 0, t))$, (b) $Im(\psi_{25}(x, y = 0, t))$, and (c) $|\psi_{25}(x, y = 0, t)|$ under the selection of free parameters related to the model and method as $p = 1, q = 1, b_1 = 1, b_2 = 5, \alpha = -0.5, \beta = 1, a = -0.5, \sigma = 1, R = 2, S = 4, E = 0, \gamma = 60^0$ in the xt-plane, and (d)-(f) 2D cross-sectional line plots of (a)-(c) at $t = 0$, respectively.

used to model physical and engineering processes, are determined to be the best at doing so. For their potential use in mathematical physics, biology, and nonlinear optics, these equations have grown significantly in importance and attraction during the past few years. Numerous definitions of fractional derivatives (FDs) have been published in the literature over the past few years to spread out the new trends in the field of fractional calculus and its practical applications in various research fields, including the modified Riemann-Liouville derivative [49], Caputo derivative [50], Local fractional derivative [51], Conformable derivative [52], Atangana-Baleanu derivative [53], Atangana-Baleanu-Riemann derivative [54], Atangana's conformable derivative [55,56], Grünwald–Letnikov derivative[57]. In the work of Tarasov [58], the author asserted that a fractional operator must adhere to the generalized Leibniz rule. Under this definition, it becomes evident that fractional derivatives characterized by non-integer orders, exemplified by the Jumarie derivative and the local derivative, are inherently incapable of meeting the requirements of the Leibniz rule. Furthermore, in their study, Cresson and Szafranska [59] delved into an extensive discussion concerning various properties associated with Jumarie's fractional derivative, as well as the local fractional derivative, within the context of a practical application. Additionally, within the same analytical framework, they discussed the chain rule property. Given the challenges in determining the most accurate fractional derivatives, this study focuses on discussing the definition and various properties of Atangana's derivative or beta derivative. Detailed information about the different FD definitions, properties, and limitations can be found in ref. [60]. Due to the unavailability of the most accurate fractional derivatives, we will discuss the definition and varieties of properties of Atangana's

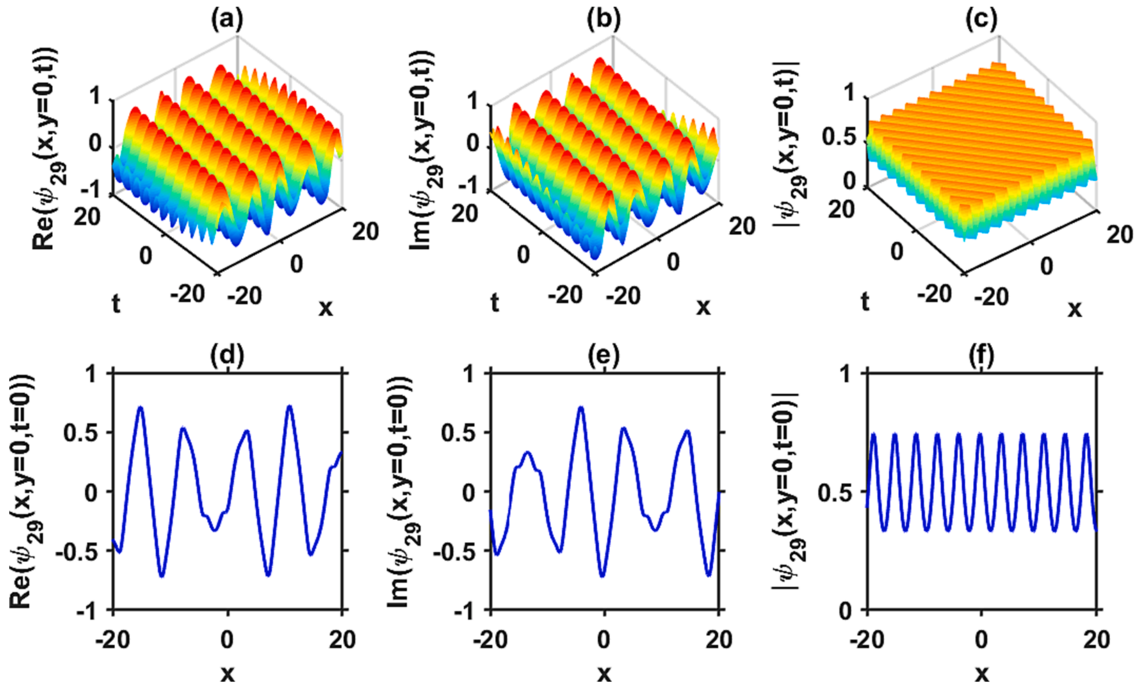

Fig. 5. Spatiotemporal illustrations of the obtained optical soliton solution given by Eq. (27) of (a) $\mathrm{Re}(\psi_{29}(x,y=0,t))$, (b) $Im(\psi_{29}(x,y=0,t))$, and (c) $|\psi_{29}(x,y=0,t)|$ under the selection of free parameters related to the model and method as $p=1, q=2, b_1=-1, b_2=-3, \alpha=1.2, \beta=-1, a=1, \sigma=1, R=5, S=5, \mathrm{E}=5, \gamma=45^0$ in the xt-plane, and (d)-(f) 2D cross-sectional line plots of (a)-(c) at $t=0$, respectively.

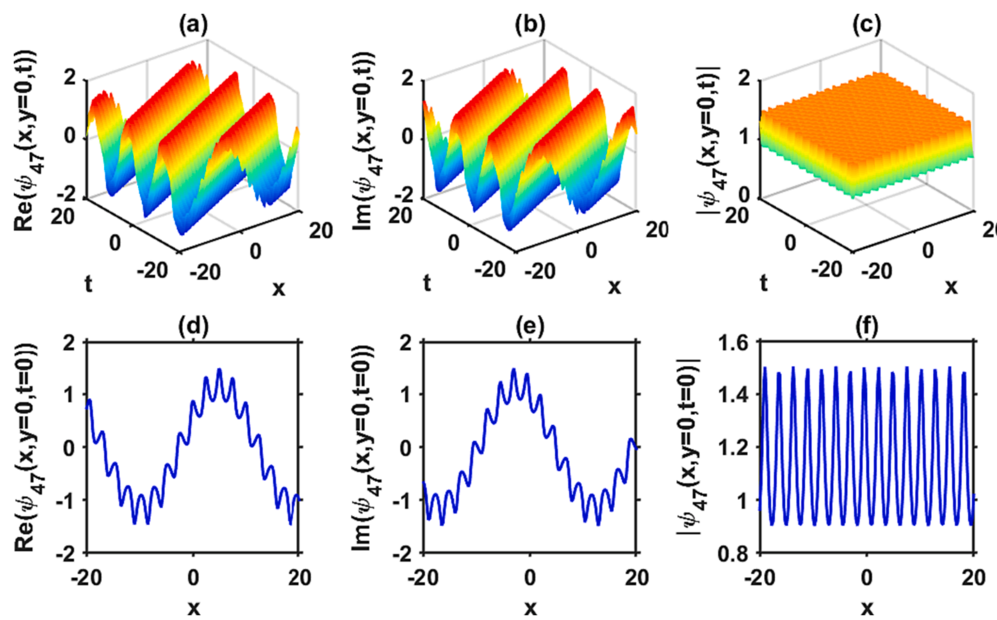

Fig. 6. Spatiotemporal illustrations of the obtained optical soliton solution given by Eq. (36) of (a) $\mathrm{Re}(\psi_{47}(x,y=0,t))$, (b) $Im(\psi_{47}(x,y=0,t))$, and (c) $|\psi_{47}(x,y=0,t)|$ under the selection of free parameters related to the model and method as $p=1, q=1, b_1=1, b_2=-1, \alpha=-0.5, \beta=1, a=-0.5, \sigma=1.5, R=2, S=-3, \mathrm{E}=-1.5, \gamma=15^0$ in the xt-plane, and (d)-(f) 2D cross-sectional line plots of (a)-(c) at $t=0$, respectively.

conformable derivative (ACD) or beta derivative. It is mentioned that the beta derivative and its properties were initially proposed by Atangana et al., [55]. Later on, Atangana and Alqahtani [56] proved that beta-derivative can describe the spread of river blindness disease model more accurately than Caputo derivative. According to merely the fundamental limit definition of the derivative, the definition of ACD as forwarded by Atangana et al., [55] is as follows:

$$ {}_0^A D_t^\tau(f(t)) = \lim_{\Delta h\to 0}\frac{f\left(t+\Delta h\left(t+\frac{1}{\Gamma(\tau)}\right)^{1-\tau}\right)-f(t)}{\Delta h}, \ for\ all\ t>0,\ 0<\tau\leqslant 1 $$

This derivative is also known as the beta derivative. In this study, the definition and characteristics of the beta derivative will be used, let us recap some of its useful properties in accordance with ref. [49] for a better perspective.

Assuming that, $a, b \in \mathbb{R}$**,** where $\mathbb{R}$ is the set of all real numbers, $g =$

$g(t) \neq 0$ and $f = f(t)$ are two functions τ-differentiable at a point $t > 0$, whereas $\tau \in (0,1]$, we have.

(i) ${}_0^AD_t^\tau(af(t) + bg(t)) = a\,{}_0^AD_t^\tau f(t) + b\,{}_0^AD_t^\tau g(t),\ \forall\, a, b \in \mathbb{R}$.

(ii) ${}_0^AD_t^\tau(C) = 0$, where C is a constant.

(iii) ${}_0^AD_t^\tau(f(t)g(t)) = g(t)\ {}_0^AD_t^\tau f(t) + f(t)\,{}_0^AD_t^\tau g(t)$.

(iv) ${}_0^AD_x^\tau\left(\frac{f(t)}{g(t)}\right) = \frac{g(t)\,{}_0^AD_x^\tau f(t) - f(t)\,{}_0^AD_t^\tau g(t)}{(g(t))^2}$.

By considering $\Delta h = \left(t + \frac{1}{\Gamma\tau}\right)^{\tau-1}h$, $h \to 0$ when $\Delta h \to 0$. Therefore, we obtain the following useful property: ${}_0^AD_t^\tau f(t) = \left(t + \frac{1}{\Gamma\tau}\right)^{\tau-1}\frac{df(t)}{dt}$.

Optical solutions of the CNS model in the presence of Atangana derivative

In recent years, a number of researchers have used the FPDEs to apply the definition of the ACD and its properties in order to obtain analytical solutions using various analytical techniques [61–64]. Being inspired by the mentioned study [61–64], we consider the following (2 + 1)-dimensional chiral NLS equation with ACD, which reads ($\tau = 1$) [28–31]:

$$i\,{}_0^AD_t^\tau\psi + a\left({}_0^AD_{xx}^{2\tau}\psi + {}_0^AD_{yy}^{2\tau}\psi\right) + i\left(b_1\left(\psi\ {}_0^AD_x^\tau\psi^* - \psi^*\,{}_0^AD_x^\tau\psi\right) + b_2\left(\psi\ {}_0^AD_y^\tau\psi^* - \psi^*\,{}_0^AD_y^\tau\psi\right)\right)\psi = 0 \tag{47}$$

where ${}_0^AD_t^\tau\psi$, ${}_0^AD_x^\tau\psi$, and ${}_0^AD_y^\tau\psi$ denote the Atangana derivative with order τ with respect to t, x, y, respectively, and $0 < \tau < 1$. The fractional-order chiral NLS equation in Eq. (47) becomes the integer-order chiral NLS equation defined by Eq. (1) when we substitute $\tau = 1$ in that equation. It is important to point out that the fractional-order (2 + 1)-dimensional chiral NLS equation should be taken into account for a number of reasons. From a literary perspective, it can be seen that, in general, the fiber also accommodates skew rays, which move at angles oblique to the fiber axis [65]. In order to describe the dynamics of oblique waves in optical fiber, the solutions resulting from such a fractional-order equation may be helpful. Additionally, the solutions can be helpful in reducing the internet bottleneck, which is a significant problem for the telecom sector [66]. Assume the following complex linear oblique transformation [67] to the (2 + 1)-dimensional chiral NLS equation with ACD:

$$Q(x,y,t;\tau) = u(\xi)e^{i\theta(x,y,t)},\ \xi = \frac{\alpha cos\gamma}{\tau}\left(x + \frac{1}{\Gamma\tau}\right)^\tau + \frac{\beta sin\gamma}{\tau}\left(y + \frac{1}{\Gamma\tau}\right)^\tau - \frac{v}{\tau}\left(t + \frac{1}{\Gamma\tau}\right)^\tau, \text{ and } \theta = \frac{pcos\gamma}{\tau}\left(x + \frac{1}{\Gamma\tau}\right)^\tau + \frac{qsin\gamma}{\tau}\left(y + \frac{1}{\Gamma\tau}\right)^\tau + \frac{w}{\tau}\left(t + \frac{1}{\Gamma\tau}\right)^\tau \tag{48}$$

With the help of the definition and feasible properties of the ACD [55], a complex linear oblique transformation specified by Eq. (48), Eq. (47) is converted to the identical ODE specified by Eq. (11). Following that, the fractional chiral NLS equation is solved using the unified method. We obtain sixty-eight (68) optical solutions that are unique in the ACD sense. For the sake of simplicity, we have included two optical solutions obtained using the unified method for Set 2 in the sense of ACD. Optical solutions to the fractional chiral NLS equation by the unified method are given below for solution Set 2: $A_0 = 0$, $A_1 = \pm\sqrt{-\frac{2T_1}{T_2}}$, $B_1 = 0$, and $w = 2T_1\sigma - T_3$.

$$\psi_{17}(x,y,t) = \sqrt{-\frac{2T_1}{T_2}}\left(\frac{\sqrt{-(R^2+S^2)\sigma} - R\sqrt{-\sigma}\cosh\left(2\sqrt{-\sigma}\left(\frac{\alpha cos\gamma}{\tau}\left(x+\frac{1}{\Gamma\tau}\right)^\tau + \frac{\beta sin\gamma}{\tau}\left(y+\frac{1}{\Gamma\tau}\right)^\tau - \frac{\left(2a\left(\alpha pcos^2\gamma+\beta qsin^2\gamma\right)\right)}{\tau}\left(t+\frac{1}{\Gamma\tau}\right)^\tau + E\right)\right)}{R\sinh\left(2\sqrt{-\sigma}\left(\frac{\alpha cos\gamma}{\tau}\left(x+\frac{1}{\Gamma\tau}\right)^\tau + \frac{\beta sin\gamma}{\tau}\left(y+\frac{1}{\Gamma\tau}\right)^\tau - \frac{\left(2a\left(\alpha pcos^2\gamma+\beta qsin^2\gamma\right)\right)}{\tau}\left(t+\frac{1}{\Gamma\tau}\right)^\tau + E\right)\right) + S}\right) \times e^{i\left(\frac{pcos\gamma}{\tau}\left(x+\frac{1}{\Gamma\tau}\right)^\tau + \frac{qsin\gamma}{\tau}\left(y+\frac{1}{\Gamma\tau}\right)^\tau + \frac{(2T_1\sigma - T_3)}{\tau}\left(t+\frac{1}{\Gamma\tau}\right)^\tau\right)} \tag{49}$$

$$\psi_{25}(x,y,t) = \sqrt{-\frac{2T_1}{T_2}}\left(\frac{\sqrt{(R^2-S^2)\sigma} - R\sqrt{\sigma}\cos\left(2\sqrt{\sigma}\left(\frac{\alpha cos\gamma}{\tau}\left(x+\frac{1}{\Gamma\tau}\right)^\tau + \frac{\beta sin\gamma}{\tau}\left(y+\frac{1}{\Gamma\tau}\right)^\tau - \frac{\left(2a\left(\alpha pcos^2\gamma+\beta qsin^2\gamma\right)\right)}{\tau}\left(t+\frac{1}{\Gamma\tau}\right)^\tau + E\right)\right)}{R\sin\left(2\sqrt{\sigma}\left(\frac{\alpha cos\gamma}{\tau}\left(x+\frac{1}{\Gamma\tau}\right)^\tau + \frac{\beta sin\gamma}{\tau}\left(y+\frac{1}{\Gamma\tau}\right)^\tau - \frac{\left(2a\left(\alpha pcos^2\gamma+\beta qsin^2\gamma\right)\right)}{\tau}\left(t+\frac{1}{\Gamma\tau}\right)^\tau + E\right)\right) + S}\right) \times e^{i\left(\frac{pcos\gamma}{\tau}\left(x+\frac{1}{\Gamma\tau}\right)^\tau + \frac{qsin\gamma}{\tau}\left(y+\frac{1}{\Gamma\tau}\right)^\tau + \frac{(2T_1\sigma - T_3)}{\tau}\left(t+\frac{1}{\Gamma\tau}\right)^\tau\right)} \tag{50}$$

where $i = \sqrt{-1}$, $T_1 = a\left(\alpha^2cos^2\gamma + \beta^2sin^2\gamma\right)$, $T_2 = 2(pb_1cos\gamma + qb_2sin\gamma)$, and $T_3 = a\left(p^2cos^2\gamma + q^2sin^2\gamma\right)$ are used for the obtained solutions given by Eqs. (49)-(50). The effects of the fractional parameter will be discussed in the results and discussion section for solutions given by Eqs. (49)-(50).

Results and discussion

In this section, the physical explanations of some of the optical solitons with fractionality, wave obliqueness, free parameters, and propagation behaviors to the integer-order and fractional-order chiral NLS equation are explained graphically. It is noted here that the graphical explanations of obtained solutions for the integer-order chiral NLS equation are discussed in the previous section. The novelty of our explored solutions via the unified method is concised in Table 1. To the best of our knowledge, the fractionalization of the chiral NLS equation in the view of Atangana derivative theory with wave obliqueness is studied for the first time.

Effect of wave obliqueness of the obtained solutions

Oblique waves can significantly reduce the amount of wave overtopping and reduce the wave loads on coastal structures compared to perpendicular waves [68]. On the other hand, in optical soliton, the fiber also accommodates skew rays, which travel at angles perpendicular to

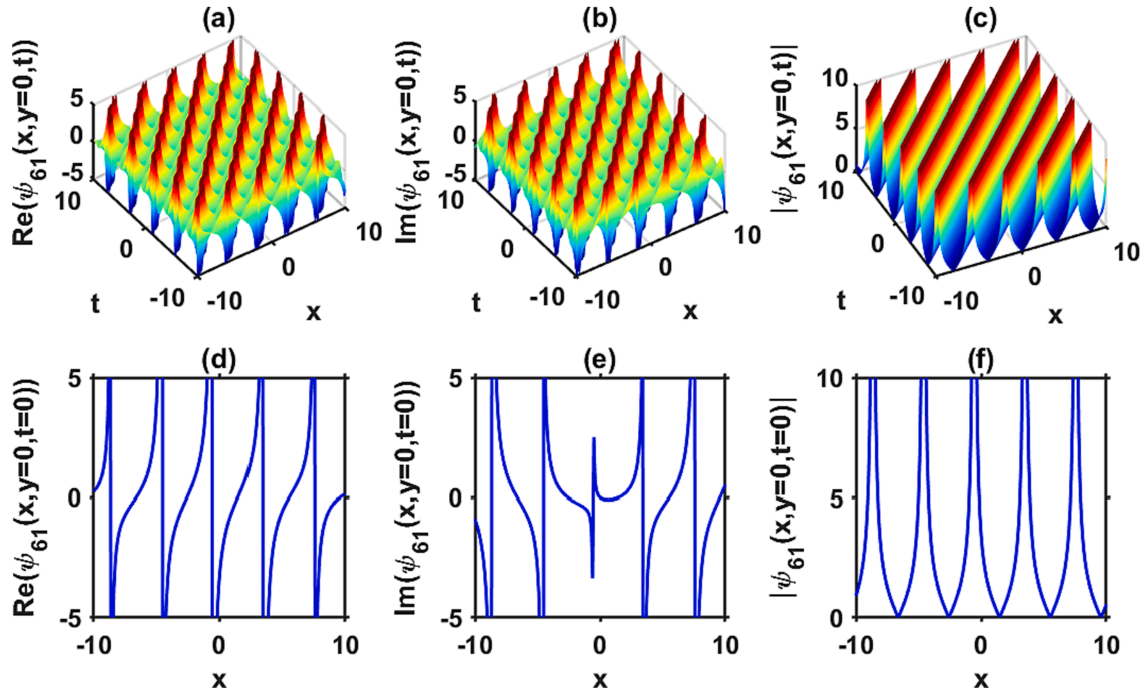

Fig. 7. Spatiotemporal illustrations of the obtained optical soliton solution given by Eq. (43) of (a) $\mathrm{Re}(\psi_{61}(x, y = 0, t))$, (b) $Im(\psi_{61}(x, y = 0, t))$, and (c) $|\psi_{61}(x, y = 0, t)|$ under the selection of free parameters related to the model and method as $p = 0.5$, $q = 0.5$, $b_1 = 1$, $b_2 = 1$, $\alpha = 1.5$, $\beta = -0.5$, $a = -1$, $\sigma = 1$, $R = -1$, $S = -1$, $\mathrm{E} = 1$, $\gamma = 75^0$ in the xt-plane, and (d)-(f) 2D cross-sectional line plots of (a)-(c) at $t = 0$, respectively.

the fiber axis [56]. Fig. 8**(a)–8(j)** and Fig. 9**(a)–9(j)** presents the effect of wave obliqueness of the CNS equation of the attained solutions given by Eq. (49) and Eq. (50), respectively when the fractional parameter $\tau = 1$. Fig. 8**(a)–8(j)** exhibit the wave obliqueness for various wave obliqueness values $\gamma = 15^\circ, 30^\circ, 45^\circ, 60^\circ, 75^\circ, 105^\circ, 120^\circ, 135^\circ, 150^\circ$ and 165°, respectively with choosing specific free parameters as $p = 1$, $q = 1$, $b_1 = 1, b_2 = 0.1, \alpha = 1.2, \beta = -1, a = 0.1, \sigma = -1, R = 1, S = 1, E = 0$, $t = 0$. On the other hand, Fig. 9**(a)–9(j)** also display the wave obliqueness for various wave obliqueness values $\gamma = 15^\circ, 30^\circ, 45^\circ, 60^\circ, 75^\circ, 105^\circ, 120^\circ, 145.05^\circ, 150^\circ$ and 165°, respectively with choosing specific free parameters as $p = 1, q = 1, b_1 = 1, b_2 = 1, \alpha = -0.5, \beta = 1, a = -0.5, \sigma = 1, R = 2, S = 4, E = 0, t = 0$. Fig. 8**(a)–8(j)** and Fig. 9 **(a)–9(j)** show that oblique waves propagate clockwise in the xy-plane, with amplitudes increasing as increases of γ for $0 < \gamma \leq 75^\circ$ and $90^\circ < \gamma \leq 165^\circ$, whereas the amplitudes are decreasing with the increase of γ for $75^\circ < \gamma < 90^\circ$ and $165^\circ < \gamma < 180^\circ$. In order to keep this study concise, the variation in oblique wave propagation with wave obliqueness of γ for $75^\circ < \gamma < 90^\circ$ and $165^\circ < \gamma < 180^\circ$ is not discussed. However, it is also evident from Fig. 8**(a)–8(j)** and Fig. 9**(a)–9(j)** that the wave profiles have changed significantly as the obliqueness has increased. The oblique wave amplitude is maximum at $\gamma = 75^\circ$ and $\gamma = 120^\circ$ in the xy-plane within the wave directions $0 < \gamma < 90^\circ$ and $90^\circ < \gamma < 180^\circ$, respectively, as can be seen from the dark profile. However, the amplitudes of smooth periodic waves reach the maximum at $\gamma = 120^\circ$ and $\gamma = 145^\circ$ in the xy-plane within the wave directions $90^\circ < \gamma < 180^\circ$ due to the change of wave shape of the solitons. It is

Table 1
A comparison between the previously published results and the solutions attained in the present study that represent the novelty of our generated solutions.

Study	What type of fractional derivative is applied?	Is wave obliqueness applied?	Reported soliton solutions to the (2 + 1)-dimensional chiral NLS equation							
			Dark shaped	Bright shaped	Kink shaped	Anti-kink shaped	Unsmooth periodic shaped	Periodic shaped	Periodic singular shaped	Singular shaped
Present study[a]	Atangana derivative	√	√	×	√	√	√	√	√	√
Sulaiman and Yusuf [33]	Not applied	×	√	√	×	×	×	√	×	√
Alshahra and Yakout [34]	Not applied	×	×	×	√	×	×	√	×	×
Akinyemi et al. [35]	Not applied	×	√	√	×	×	×	√	×	√
Ghanbari and Gómez-Aguilar [36]	Conformable derivative	×	×	×	√	×	×	×	√	×
Awan and Tahir [37]	Not applied	×	√	×	×	×	×	×	√	√
Wang and Wang [38]	Not applied	×	×	√	√	×	×	√	×	×

Note: [a]The unified method. The symbol √ represents that the wave obliqueness is applied and the indicated solitons are reported, and the symbol × represents that the wave obliqueness is not applied and the indicated solitons are not reported.

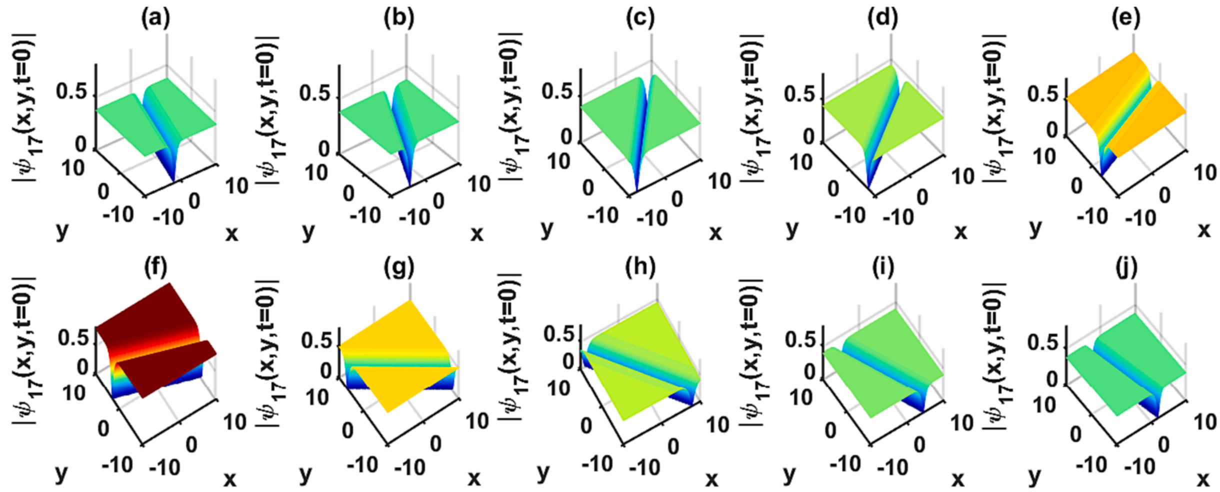

Fig. 8. Effects of wave obliqueness of the attained solution $|\psi_{17}(x,y,t=0;\gamma)|$ with $\tau=1$ given by Eq. (49): (a)-(j) $\gamma=15^{\circ},30^{\circ},45^{\circ},60^{\circ},75^{\circ},105^{\circ},120^{\circ},135^{\circ},150^{\circ},165^{\circ}$, respectively under choosing specific free parameters as $p=1$, $q=1$, $b_1=1$, $b_2=0.1$, $\alpha=1.2$, $\beta=-1$, $a=0.1$, $\sigma=-1$, $R=1$, $S=1$, $E=0$, $t=0$.

mentioned that the reported periodic, unsmooth periodic, singular periodic shaped, and other solitons exhibit the same pattern as the dark and equal wave length periodic solitons. All figures are not presented due to the simplicity and briefness of the manuscript.

Effect of fractionality of the obtained solutions

Optical soliton solutions combined with wave obliqueness and fractionality to the fractional-order chiral NLS equation are obtained via the unified method. To illustrate the effects of the fractional parameter of the attained solutions $|\psi_{17}(x,y=0,t;\gamma=60^{\circ},\tau)|$ and $|\psi_{25}(x,y=0,t;\gamma=15^{\circ},\tau)|$ given by Eq. (49) and Eq. (50), the spatiotemporal variations are presented in Fig. 10**(a)-(e)** and Fig. 11**(a)-(e) through 3D** graphs, respectively under the consideration of different fractional values ($\tau=0.15, 0.25, 0.50, 0.75, 0.95$). For preparing Fig. 10, the selected free parameters are $p=1$, $q=1$, $b_1=1$, $b_2=0.1$, $\alpha=1.2$, $\beta=-1$, $a=0.1$, $\sigma=-1$, $R=1$, $S=1$, $E=0$ for solution $|\psi_{17}(x,y=0,t;\gamma=60^{\circ},\tau)|$. On the other hand, for preparing Fig. 10, the selected parameters are $p=1$, $q=1$, $b_1=1$, $b_2=1$, $\alpha=-0.5$, $\beta=1$, $a=-0.5$, $\sigma=1$, $R=2$, $S=4$, $E=0$ for solution $|\psi_{25}(x,y=0,t;\gamma=15^{\circ},\tau)|$. The 2D cross-sectional plot along x-axis at $t=0$ for these mentioned solutions are shown in Fig. 10**(f) and** Fig. 11 **(f)**, respectively for the consideration of different fractional values ($\tau=0.15, 0.25, 0.50, 0.75, 0.95$). It can be seen from Fig. 10**(f)** that the surface wave profiles along the x-axis are not a complete form of dark for $\tau=0.15$,0.25,0.50,0.75. However, the amplitudes are slightly increased with the increase of the fractional parameter. Moreover, the profile completes the forms of a dark soliton when we choose $\tau=0.95$. It can be also seen from Fig. 11**(f)** that the number of oscillations of the periodic wave increases with the increase of fractional parameters. However, it is discovered that the wave profiles' amplitudes for the various values of $\tau=0.15$, 0.25, 0.50, 0.75, and 0.95 are nearly identical, but they change into the x-axis. It is previously mentioned that the above solutions represent the dark and periodic profiles when we consider $\tau=1$.

Effects of free parameters with model and transformation

For dark and periodic solitons Fig. 12**(a)-12(c)** and Fig. 14 **(a)-14(c)** represent the effects of free parameters b_1, b_2, and a of the chiral NLS model equation, and Fig. 13**(a)-13(d)** and Fig. 15**(a)-15(d)** represent

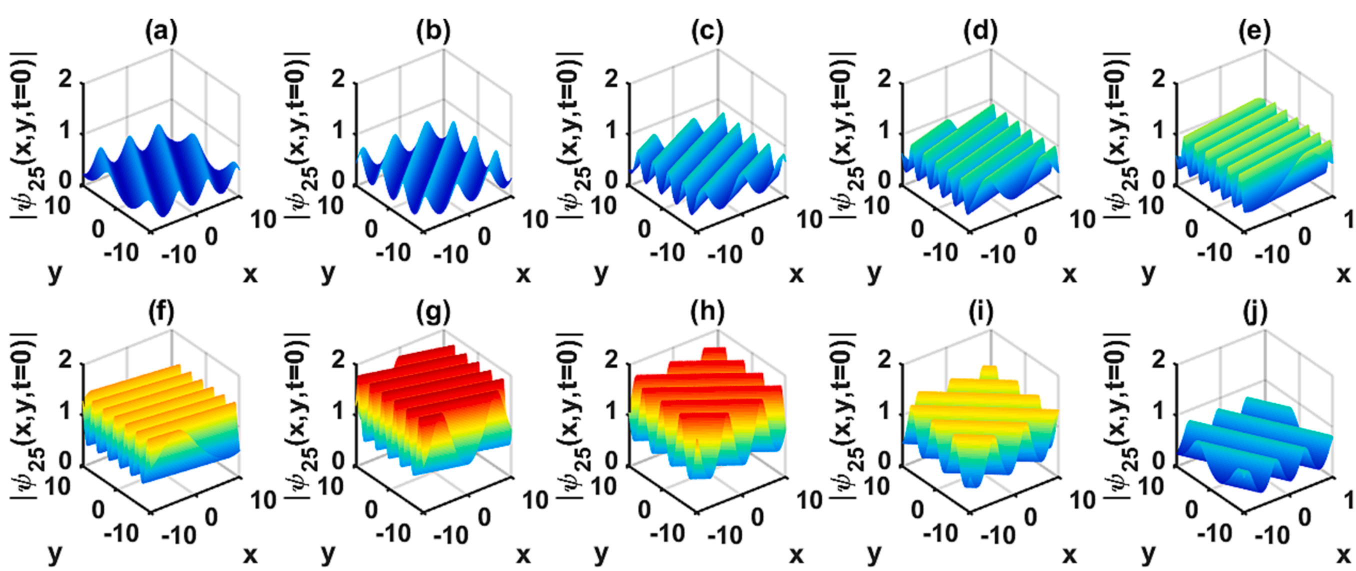

Fig. 9. Effects of wave obliqueness of the attained solution $|\psi_{25}(x,y,t=0;\gamma)|$ with $\tau=1$ given by Eq. (50): (a)-(j) $\gamma=15^{\circ},30^{\circ},45^{\circ},60^{\circ},75^{\circ},105^{\circ},120^{\circ},145^{\circ},150^{\circ},165^{\circ}$, respectively with choosing specific free parameters as $p=1$, $q=1$, $b_1=1$, $b_2=1$, $\alpha=-0.5$, $\beta=1$, $a=-0.5$, $\sigma=1$, $R=2$, $S=4$, $E=0$, $t=0$.

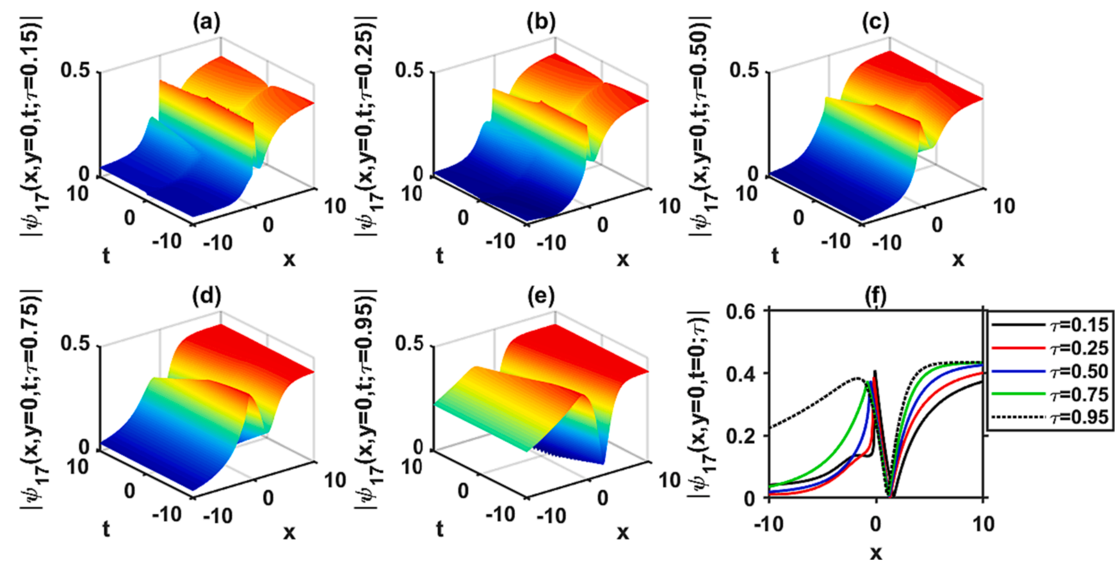

Fig. 10. Effects of the fractionality on the obtained solution $|\psi_{17}(x, y = 0, t; \gamma = 60^{\circ}, \tau)|$ given by Eq. (49): (a)-(e) $\tau = 0.15, 0.25, 0.50, 0.75, 0.95$, respectively for choosing specific free parameters as $p = 1$, $q = 1$, $b_1 = 1$, $b_2 = 0.1$, $\alpha = 1.2$, $\beta = -1$, $a = 0.1$, $\sigma = -1$, $R = 1$, $S = 1$, $E = 0$, $y = 0$, and (f) the variation of the 2D cross-sectional plots of (a)-(e) at $t = 0$.

the effects of free parameters p, q, α, and β transformations of the chiral NLS mode equation. In Fig. 12**(a)**, it can be seen that the soliton profiles along the x-axis are changed for all values of the free parameter $b_1 = 1$, 2, 4. Fig. 12**(a)** demonstrates that the amplitude decreases as the increases of the values b_1 and the phase component is also changed. Similar tendencies have been found for the values of $b_2 = 0.1, 0.5, 0.9$, $p = 1, 2, 4$ and $q = 1, 2, 4$, which are shown in Fig. 12**(b),** Fig. 13**(a),** and Fig. 13**(b),** respectively. Fig. 12**(c)** represents the different values of $a =$ 0.25, 0.50, 0.75 and 1. From Fig. 12**(c),** it is visible that the amplitude increases as the increases the values of a. Similar tendencies have been found for the values of $\beta = 0.25$, 0.50, 0.75, and 1, which is shown in Fig. 13**(d).** Fig. 13**(c)** when the value of a $(-0.75, -0.25)$ increases the amplitude propagation toward the negative direction of x-axis. Similarly, the value of a $(0.25, 0.75)$ increases the amplitude and also propagates toward the negative direction of x-axis. From Fig. 14**(a),** it is visible that the amplitude gradually decreases as the increases of the values $b_1 = 1, 2, 3$ which propagate toward the positive direction of x-axis. A similar propensity has been found for the values of $b_2 = 1, 2, 3$, $a = -0.3, -0.2, -0.1$, $p = 1, 2, 3$, $q = 1, 3, 5$, and $\alpha = -0.6, -0.5, -0.4$, which are shown in Fig. 14**(b),** Fig. 14**(c),** Fig. 15**(a),** Fig. 15**(b)** and Fig. 15**(c),** respectively. In Fig. 15**(d),** the amplitude gradually increases as the increases of values $\beta = 0.2, 0.8, 1.4$.

Wave propagation behaviors of the obtained optical solutions

Fig. 16 shows the propagation behavior of the dark soliton solution $|\psi_{17}(x, y, t, \gamma = 60^{\circ})|$ for a sequence of times $t = -30, -20, -10, 0, 10, 20, 30$. The dark soliton's position in the xy-plane changes as time (t) rises, as can be seen in Fig. 16**(a)-16(g)**. However, the shape of the soliton and its amplitude remain unchanged. By examining its cross-

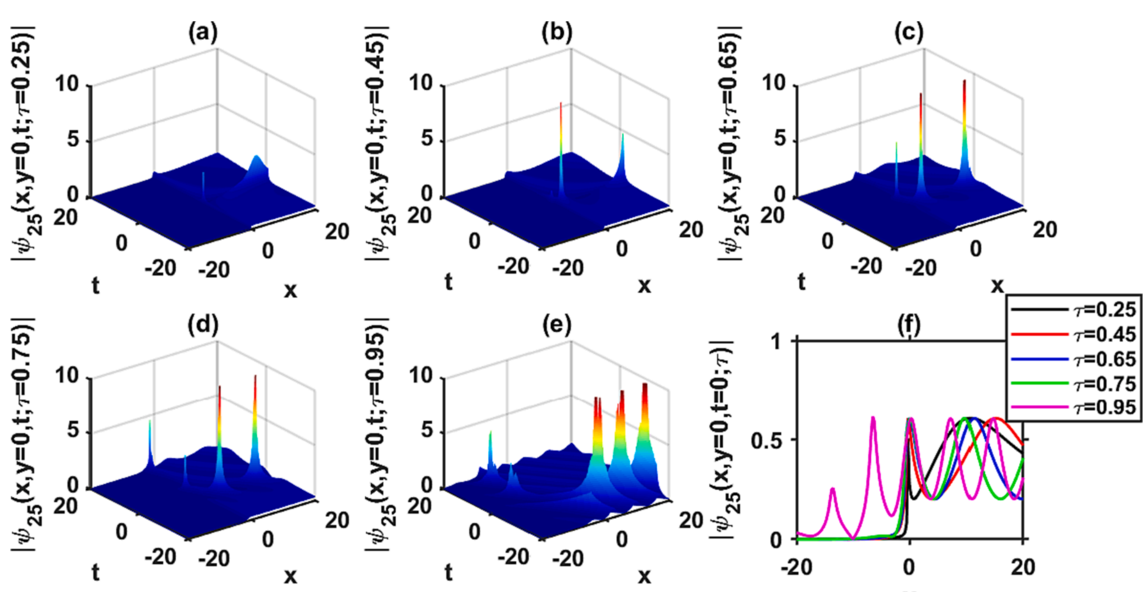

Fig. 11. Effects of the fractionality on the obtained solution $|\psi_{25}(x, y = 0, t; \gamma = 15^{\circ}, \tau)|$ given by Eq. (50): (a)-(e) $\tau = 0.25, 0.45, 0.65, 0.75, 0.95$, respectively for choosing specific free parameters as $p = 1$, $q = 1$, $b_1 = 1$, $b_2 = 1$, $\alpha = -0.5$, $\beta = 1$, $a = -0.5$, $\sigma = 1$, $R = 2$, $S = 4$, $E = 0$, $y = 0$, and (f) the variation of the 2D cross-sectional plots of (a)-(e) at $t = 0$.

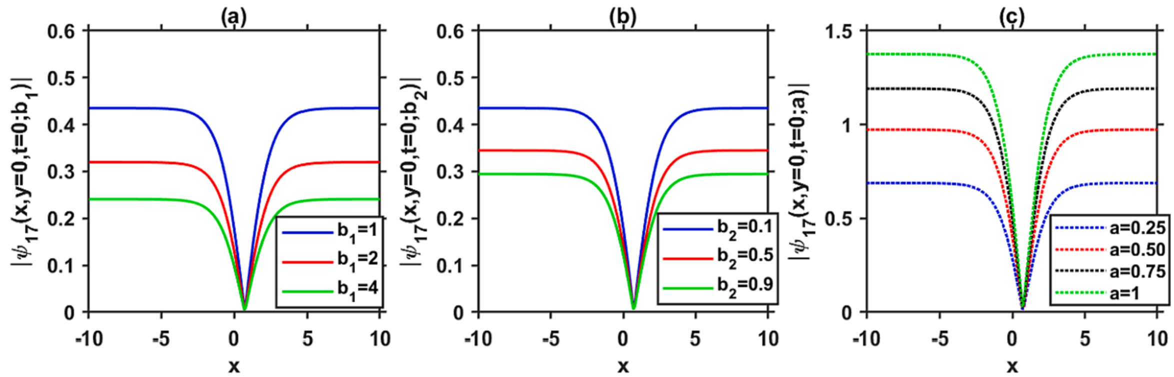

Fig. 12. Effects of the free parameters on the chiral NLS equation for the obtained solution given by $|\psi_{17}(x, y = 0, t = 0, \gamma = 60^{\circ})|$: (a) b_1 when $p = 1,\ q = 1,\ b_2 = 0.1,\ \alpha = 1.2,\ \beta = -1,\ a = 0.1,\ \sigma = -1,\ R = 1,\ S = 1,\ E = 0$, (b) b_2 when $p = 1,\ q = 1,\ b_1 = 1,\ \alpha = 1.2,\ \beta = -1,\ a = 0.1,\ \sigma = -1,\ R = 1,\ S = 1,\ E = 0$, (c) a when $p = 1,\ q = 1,\ b_1 = 1,\ b_2 = 0.1,\ \alpha = 1.2,\ \beta = -1,\ a = 0.1,\ \sigma = -1,\ R = 1,\ S = 1,\ E = 0$.

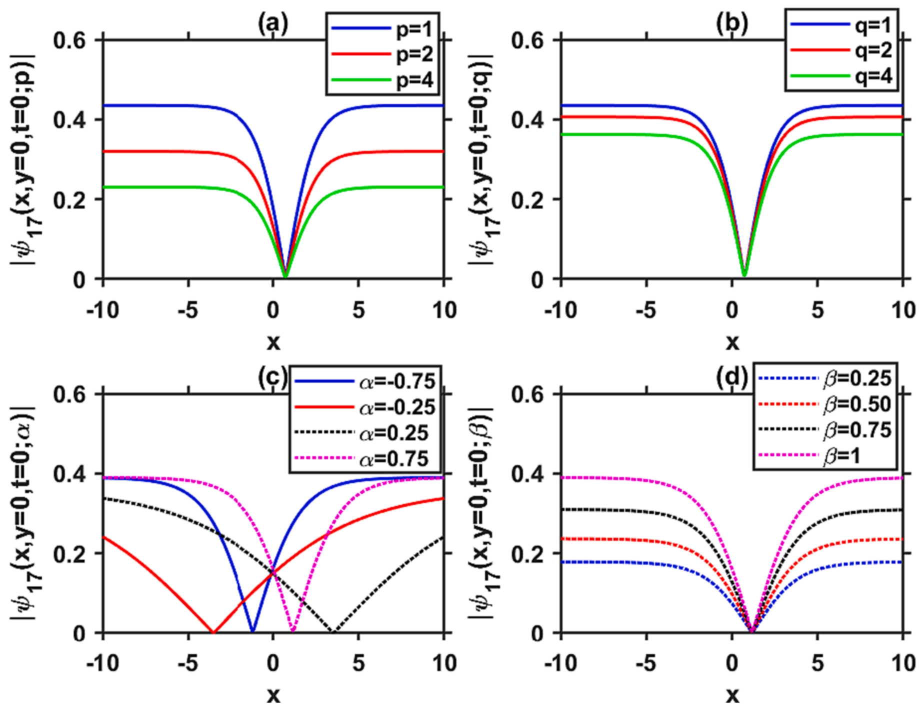

Fig. 13. Effects of the free parameters on the transformations of the chiral NLS equation for the obtained solution given by $|\psi_{17}(x, y = 0, t = 0, \gamma = 60^{\circ})|$: (a)$p$ when $q = 1,\ b_1 = 1,\ b_2 = 0.1,\ \alpha = 1.2,\ \beta = -1,\ a = 0.1,\ \sigma = -1,\ R = 1,\ S = 1,\ E = 0$, (b)$q$ when $p = 1,\ b_1 = 1,\ b_2 = 0.1,\ \alpha = 1.2,\ \beta = -1,\ a = 0.1,\ \sigma = -1,\ R = 1,\ S = 1,\ E = 0$, (c),$\alpha$ when $p = 1,\ q = 1,\ b_1 = 1,\ b_2 = 0.1,\ \beta = -1,\ a = 0.1,\ \sigma = -1,\ R = 1,\ S = 1,\ E = 0$, (d)$\beta$ when $p = 1,\ q = 1,\ b_1 = 1,\ b_2 = 0.1,\ \alpha = 1.2,\ a = 0.1,\ \sigma = -1,\ R = 1,\ S = 1,\ E = 0$.

sectional plots along $y = 0$ at different times $t = -30, -20, -10, 0, 10, 20, 30$, the dark soliton's aforementioned propagation behavior is validated. The soliton is propagating from the positive side of the x-axis to its negative side with an increase of time, as can also be observed from Fig. 16**(h)**. For a sequence of times $t = -9, -6, -3, 0, 3, 6, 9$ and assuming the free parameters as $p = 1,\ q = 1,\ b_1 = 1,\ b_2 = 1,\ \alpha = -0.5,\ \beta = 1,\ a = -0.5,\ \sigma = 1,\ R = 2,\ S = 4,\ E = 0$, the propagation behaviour of the periodic soliton solution $|\psi_{25}(x, y, t, \gamma = 45^{\circ})|$ is shown in Fig. 17. As time (t) increases, the position of the dark soliton in the $xy-$ plane changes, as shown in Fig. 17**(a)-17(g)**. The propagation behavior of the dark soliton at different times $t = -9, -6, -3, 0, 3, 6, 9$ is validated by its cross-sectional plots along $y = 0$. The soliton propagates with increasing time from the negative side of the x-axis to its positive side, as shown in Fig. 17**(h)** as well.

Conclusions

The $(2 + 1)$-dimensional chiral NLS equation equation is examined in this study in order to discover some innovative soliton solutions and wave obliqueness using the unified method. The key findings of this investigation are presented here. The unified method yields dark, periodic singular with unequal wavelength, periodic with equal wavelength, periodic, unsmooth periodic, and singular periodic soliton solutions which are presented in Figs. 1-7. The applied methods have also added some novel oblique wave solitons to the investigated equation. As the obliqueness and fractionality change, it has been shown that the wave profile also changes. The 3D graphical illustrations and 2D cross-sectional graphics for different values of various parameters are represented to understand the effects of the changing values of the parameters on the attained solutions. Figs. 8-9 provide a graphic illustration of the impact of wave obliqueness on the dark and periodic soliton. Due to

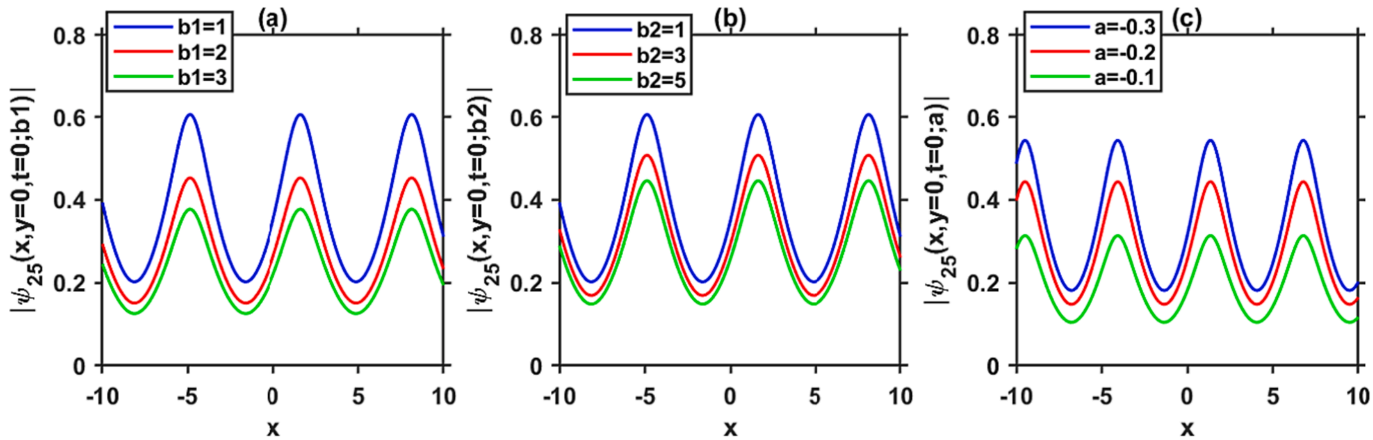

Fig. 14. Effects of the free parameters on the chiral NLS equation for the obtained solution given by $|\psi_{25}(x, y = 0, t = 0, \gamma = 15^{\circ})|$: (a) b_1 when $p = 1, q = 1, b_2 = 1, \alpha = -0.5, \beta = 1, a = -0.5, \sigma = 1, R = 2, S = 4, E = 0$, (b) b_2 when $p = 1, q = 1, b_1 = 1, \alpha = -0.5, \beta = 1, a = -0.5, \sigma = 1, R = 2, S = 4, E = 0$, (c) a when $p = 1, q = 1, b_1 = 1, b_2 = 1, \alpha = -0.5, \beta = 1, \sigma = 1, R = 2, S = 4, E = 0$.

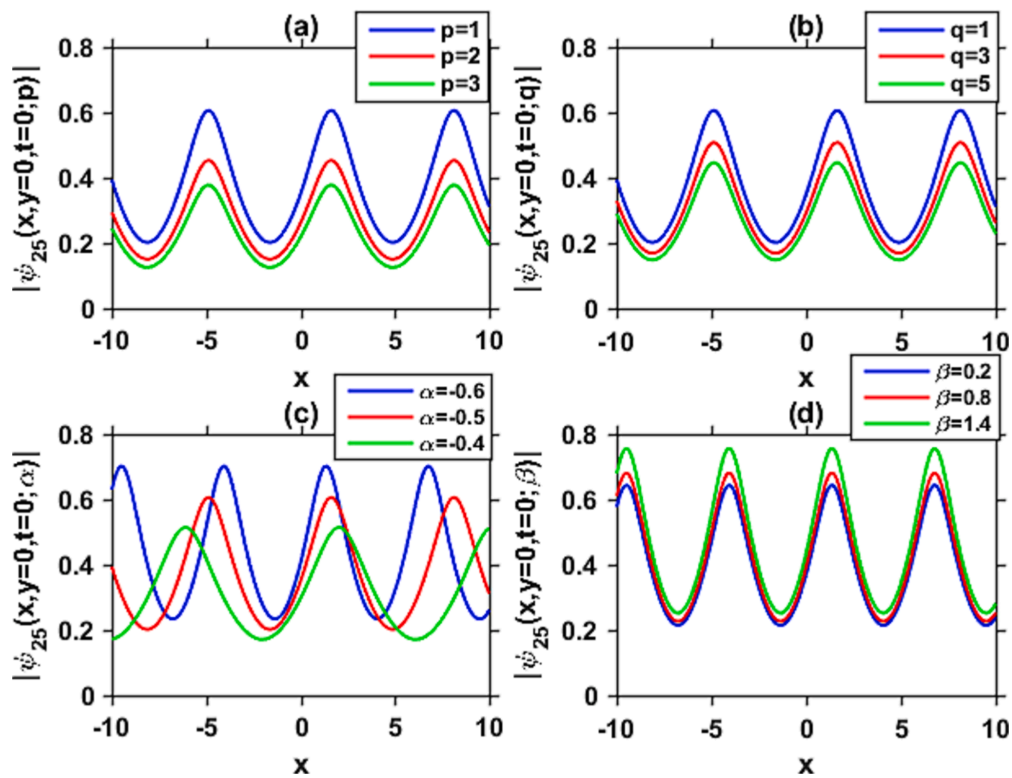

Fig. 15. Effects of the free parameters on the transformations of the chiral NLS equation for the obtained solution given by $|\psi_{25}(x, y = 0, t = 0, \gamma = 15^{\circ})|$: (a) p when $q = 1, b_1 = 1, b_2 = 1, \alpha = -0.5, \beta = 1, a = -0.5, \sigma = 1, R = 2, S = 4, E = 0$, (b) q when $p = 1, b_1 = 1, b_2 = 1, \alpha = -0.5, \beta = 1, a = -0.5, \sigma = 1, R = 2, S = 4, E = 0$, (c) α when $p = 1, q = 1, b_1 = 1, b_2 = 1, \beta = 1, a = -0.5, \sigma = 1, R = 2, S = 4, E = 0$, (d) β when $p = 1, q = 1, b_1 = 1, b_2 = 1, \alpha = -0.5, a = -0.5, \sigma = 1, R = 2, S = 4, E = 0$.

the increase in wave obliqueness γ ($0 < \gamma < 90^{\circ}$ and $90^{\circ} < \gamma < 180^{\circ}$), it is discovered that the soliton rotates in a clockwise manner. The effects of fractionality are presented in Figs. 10-11. On the other hand, Figs. 12-15 show the cross-sectional plots and physical descriptions of the impacts of the free parameters $(a, \alpha, \beta, b_1, b_2, p, q)$ on the investigated dark and periodic solitons. It is discovered that the dark and periodic soliton profiles change as the free parameters change. As time increases, all the attained solitons propagate in the *xy*-plane. The wave propagation behaviors of the obtained solutions are explained graphically in Figs. 16-17. The summarized results indicate that the wave propagation of solitons is controlled by the free parameters and wave obliqueness. The described solitons can also be utilized to explain the wave propagation behaviors in physical and telecommunication systems, which is another significant point to emphasize here. Therefore, the obtained optical solutions could assist the researchers in further investigations to explain unknown wave approaching obliqueness in the field of fiber optics and optical communications.

Compliance with ethical standards

This article does not contain any studies with human or animal subjects.

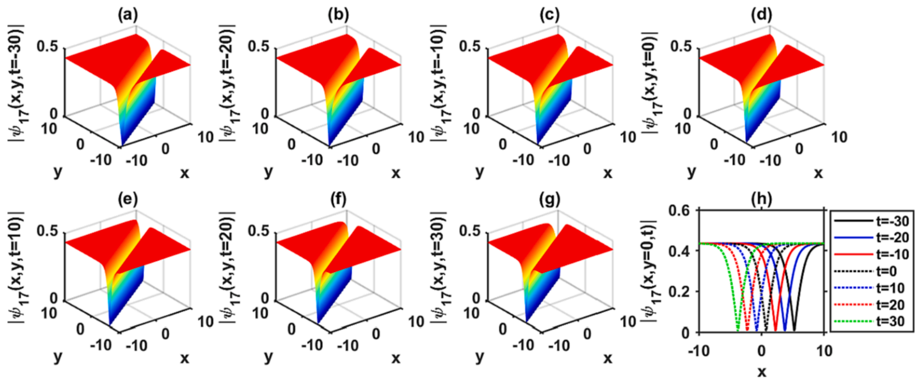

Fig. 16. Effects of the propagation behaviors on the obtained solution given by $|\psi_{17}(x,y,t,\gamma = 60^{\circ})|$: (a)-(g) $t = -30,\ -20,\ -10,\ 0,\ 10,\ 20,\ 30$, respectively, for choosing specific free parameters as $p = 1,\ q = 1,\ b_1 = 1,\ b_2 = 0.1,\ \alpha = 1.2,\ \beta = -1,\ a = 0.1,\ \sigma = -1,\ R = 1,\ S = 1,\ E = 0$, and (f) the variation of cross sectional 2D line plots of (a)-(g) at $y = 0$.

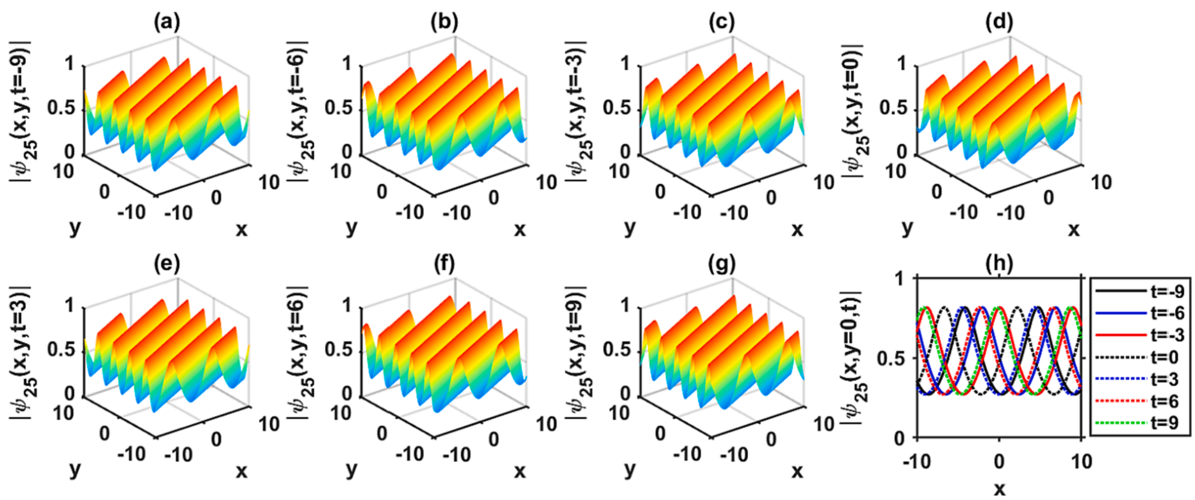

Fig. 17. Effects of the propagation behaviors on the obtained solution given by $|\psi_{25}(x,y,t,\gamma = 45^{\circ})|$: (a)-(g) $t = -9,\ -6,\ -3,\ 0,\ 3,\ 6,\ 9$, respectively, for choosing specific free parameters as $p = 1,\ q = 1,\ b_1 = 1,\ b_2 = 1,\ \alpha = -0.5,\ \beta = 1,\ a = -0.5,\ \sigma = 1,\ R = 2,\ S = 4,\ E = 0$, and (f) the variation of cross sectional 2D line plots of (a)-(g) at $y = 0$.

CRediT authorship contribution statement

K.M. Abdul Al Woadud: Methodology, Formal analysis, Software, Validation, Writing – original draft. **Dipankar Kumar:** Formal analysis, Software, Supervision, Conceptualization, Data curation, Resources, Validation, Writing - review & editing. **Aminur Rahman Khan:** Formal analysis, Resources, Supervision, Writing – review & editing.

Declaration of Competing Interest

The authors declare that they have no known competing financial interests or personal relationships that could have appeared to influence the work reported in this paper.

Data availability

Data will be made available on request.

Acknowledgment

The authors are grateful to the editor and two anonymous referees for their careful reading of our manuscript and their insightful comments and useful suggestions that helped us to improve the article.

References

[1] Wang M, Zhou Y, Li Z. Application of a homogeneous balance method to exact solutions of nonlinear equations in mathematical physics. Phys Lett A 1996 Jun 17; 216(1–5):67–75.
[2] Abdou MA. The extended F-expansion method and its application for a class of nonlinear evolution equations. Chaos Solitons Fractals 2007 Jan 1;31(1):95–104.
[3] Fan E. Extended tanh-function method and its applications to nonlinear equations. Phys Lett A 2000 Dec 4;277(4–5):212–8.
[4] Hossain AK, Akbar MA, Azad MA. Closed form wave solutions of two nonlinear evolution equations. Cogent Physics 2017 Jan 1;4(1):1396948.
[5] Zayed EM, Gepreel KA. The (G′/G)-expansion method for finding traveling wave solutions of nonlinear partial differential equations in mathematical physics. J Math Phys 2009 Jan 1;50(1).
[6] Ma WX, Lee JH. A transformed rational function method and exact solutions to the 3+ 1 dimensional Jimbo-Miwa equation. Chaos Solitons Fractals 2009 Nov 15;42 (3):1356–63.
[7] Khater MM, Kumar D. New exact solutions for the time fractional coupled Boussinesq-Burger equation and approximate long water wave equation in shallow water. J Ocean Eng Sci 2017 Sep 1;2(3):223–8.
[8] Akbulut A, Kaplan M. Auxiliary equation method for time-fractional differential equations with conformable derivative. Comput Math Appl 2018 Feb 1;75(3): 876–82.
[9] Chen Y, Yan Z. The Weierstrass elliptic function expansion method and its applications in nonlinear wave equations. Chaos Solitons Fractals 2006 Aug 1;29 (4):948–64.
[10] Hosseini K, Samadani F, Kumar D, Faridi M. New optical solitons of cubic-quartic nonlinear Schrödinger equation. Optik 2018 Mar;1(157):1101–5.
[11] Kumar D, Seadawy AR, Joardar AK. Modified Kudryashov method via new exact solutions for some conformable fractional differential equations arising in mathematical biology. Chin J Phys 2018 Feb 1;56(1):75–85.

[12] Kumar D, Darvishi MT, Joardar AK. Modified Kudryashov method and its application to the fractional version of the variety of Boussinesq-like equations in shallow water. Opt Quant Electron 2018 Mar;50:1–7.
[13] Joardar AK, Kumar D, Al Woadud KA. New exact solutions of the combined and double combined sinh-cosh-Gordon equations via modified Kudryashov method. Int J Phys Res 2018;1:25–30.
[14] Kumar D, Hosseini K, Samadani F. The sine-Gordon expansion method to look for the traveling wave solutions of the Tzitzéica type equations in nonlinear optics. Optik 2017 Nov;1(149):439–46.
[15] Kumar D, Seadawy AR, Chowdhury R. On new complex soliton structures of the nonlinear partial differential equation describing the pulse narrowing nonlinear transmission lines. Opt Quant Electron 2018 Feb;50:1–4.
[16] Kumar D, Manafian J, Hawlader F, Ranjbaran A. New closed form soliton and other solutions of the Kundu-Eckhaus equation via the extended sinh-Gordon equation expansion method. Optik 2018 May;1(160):159–67.
[17] Foroutan M, Kumar D, Manafian J, Hoque A. New explicit soliton and other solutions for the conformable fractional Biswas-Milovic equation with Kerr and parabolic nonlinearity through an integration scheme. Optik 2018 Oct;1(170): 190–202.
[18] Seadawy AR, Kumar D, Chakrabarty AK. Dispersive optical soliton solutions for the hyperbolic and cubic-quintic nonlinear Schrödinger equations via the extended sinh-Gordon equation expansion method. The European Physical Journal plus 2018 May 1;133(5):182.
[19] Seadawy AR, Kumar D, Hosseini K, Samadani F. The system of equations for the ion sound and Langmuir waves and its new exact solutions. Results Phys 2018 Jun;1 (9):1631–4.
[20] Geng KL, Zhu BW, Cao QH, Dai CQ, Wang YY. Nondegenerate soliton dynamics of nonlocal nonlinear Schrödinger equation. Nonlinear Dyn 2023 Sep;111(17): 16483–96.
[21] Ullah N, Asjad MI, Ur Rehman H, Akgül A. Construction of optical solitons of Radhakrishnan–Kundu–Lakshmanan equation in birefringent fibers. Nonlinear Eng 2022 Mar 24;11(1):80–91.
[22] Asjad MI, Ullah N, Rehman HU, Gia TN. Novel soliton solutions to the Atangana-Baleanu fractional system of equations for the ISALWs. Open Phys 2021 Dec 13;19 (1):770–9.
[23] Rehman HU, Inc M, Asjad MI, Habib A, Munir Q. New soliton solutions for the space-time fractional modified third order Korteweg–de Vries equation. J Ocean Eng Sci 2022 May 25.
[24] Rehman HU, Iqbal I, Zulfiqar H, Gholami D, Rezazadeh H. Stochastic soliton solutions of conformable nonlinear stochastic systems processed with multiplicative noise. Phys Lett A 2023 Oct;28(486):129100.
[25] Kudryashov NA. Seven common errors in finding exact solutions of nonlinear differential equations. Commun Nonlinear Sci Numer Simul 2009 Sep 1;14(9–10): 3507–29.
[26] Kudryashov NA, Loguinova NB. Be careful with the Exp-function method. Commun Nonlinear Sci Numer Simul 2009 May 1;14(5):1881–90.
[27] Kudryashov NA. On "new travelling wave solutions" of the KdV and the KdV–Burgers equations. Commun Nonlinear Sci Numer Simul 2009 May 1;14(5): 1891–900.
[28] Raza N, Javid A. Optical dark and dark-singular soliton solutions of (1+ 2)-dimensional chiral nonlinear Schrodinger's equation. Waves Random Complex Media 2019 Jul 3;29(3):496–508.
[29] Bulut H, Sulaiman TA, Demirdag B. Dynamics of soliton solutions in the chiral nonlinear Schrödinger equations. Nonlinear Dyn 2018 Feb;91:1985–91.
[30] Younis M, Cheemaa N, Mahmood SA, Rizvi ST. On optical solitons: the chiral nonlinear Schrödinger equation with perturbation and Bohm potential. Opt Quant Electron 2016 Dec;48:1–4.
[31] Eslami M. Trial solution technique to chiral nonlinear Schrodinger's equation in (1 + 2)-dimensions. Nonlinear Dyn 2016 Jul;85(2):813–6.
[32] Albosaily S, Mohammed WW, Aiyashi MA, Abdelrahman MA. Exact solutions of the (2+ 1)-dimensional stochastic chiral nonlinear Schrödinger equation. Symmetry 2020 Nov 14;12(11):1874.
[33] Sulaiman TA, Yusuf A, Abdel-Khalek S, Bayram M, Ahmad H. Nonautonomous complex wave solutions to the (2+ 1)-dimensional variable-coefficients nonlinear Chiral Schrödinger equation. Results Phys 2020 Dec;1(19):103604.
[34] Alshahrani B, Yakout HA, Khater MM, Abdel-Aty AH, Mahmoud EE, Baleanu D, et al. Accurate novel explicit complex wave solutions of the (2+ 1)-dimensional Chiral nonlinear Schrödinger equation. Results Phys 2021 Apr;1(23):104019.
[35] Akinyemi L, Inc M, Khater MM, Rezazadeh H. Dynamical behaviour of Chiral nonlinear Schrödinger equation. Opt Quant Electron 2022 Mar;54(3):191.
[36] Ghanbari B, Gómez-Aguilar JF, Bekir A. Soliton solutions in the conformable (2+ 1)-dimensional chiral nonlinear Schrödinger equation. J Opt 2022 Jun;51(2): 289–316.
[37] Awan AU, Tahir M, Abro KA. Multiple soliton solutions with chiral nonlinear Schrödinger's equation in (2+ 1)-dimensions. European Journal of Mechanics-B/ fluids 2021 Jan;1(85):68–75.
[38] Wang KJ, Wang GD. Variational theory and new abundant solutions to the (1+ 2)-dimensional chiral nonlinear Schrödinger equation in optics. Phys Lett A 2021 Oct; 7(412):127588.
[39] Nishino A, Umeno Y, Wadati M. Chiral nonlinear Schrödinger equation. Chaos Solitons Fractals 1998 Jul 1;9(7):1063–9.
[40] Gözükızıl ÖF, Akçağıl Ş, Aydemir T. Unification of all hyperbolic tangent function methods. Open Physics 2016 Jan 1;14(1):524–41.
[41] Akcagil S, Aydemir T. A new application of the unified method. New Trends in Mathematical Sciences 2018.
[42] Malfliet W, Hereman W. The tanh method: I. Exact solutions of nonlinear evolution and wave equations. Phys Scr 1996.
[43] Elwakil SA, El-Labany SK, Zahran MA, Sabry R. Modified extended tanh-function method and its applications to nonlinear equations. Appl Math Comput 2005 Feb 15;161(2):403–12.
[44] Khuri SA. A complex tanh-function method applied to nonlinear equations of Schrödinger type. Chaos Solitons Fractals 2004 Jun 1;20(5):1037–40.
[45] Wang M, Li X, Zhang J. The (G′ G)-expansion method and travelling wave solutions of nonlinear evolution equations in mathematical physics. Phys Lett A 2008 Jan 21; 372(4):417–23.
[46] Zhang J, Wei X, Lu Y. A generalized (G′ G)-expansion method and its applications. Phys Lett A 2008 May 12;372(20):3653–8.
[47] Nuruzzaman M, Kumar D, Paul GC. Fractional low-pass electrical transmission line model: Dynamic behaviors of exact solutions with the impact of fractionality and free parameters. Results Phys 2021 Aug;1(27):104457.
[48] Kumar D, Paul GC. Solitary and periodic wave solutions to the family of nonlinear conformable fractional Boussinesq-like equations. Mathematical Methods in the Applied Sciences 2021 Mar 15;44(4):3138–58.
[49] Jumarie G. Modified Riemann-Liouville derivative and fractional Taylor series of nondifferentiable functions further results. Comput Math Appl 2006 May 1;51 (9–10):1367–76.
[50] Bonyah E, Atangana A, Khan MA. Modeling the spread of computer virus via Caputo fractional derivative and the beta-derivative. Asia Pacific Journal on Computational Engineering 2017 Dec;4:1–5.
[51] Khalil R, Al Horani M, Yousef A, Sababheh M. A new definition of fractional derivative. J Comput Appl Math 2014 Jul;1(264):65–70.
[52] Abdeljawad T. On conformable fractional calculus. J Comput Appl Math 2015 May; 1(279):57–66.
[53] Bas E, Ozarslan R. Real world applications of fractional models by Atangana-Baleanu fractional derivative. Chaos Solitons Fractals 2018 Nov;1(116):121–5.
[54] Khater MM, Ghanbari B, Nisar KS, Kumar D. Novel exact solutions of the fractional Bogoyavlensky-Konopelchenko equation involving the Atangana-Baleanu-Riemann derivative. Alex Eng J 2020 Oct 1;59(5):2957–67.
[55] Atangana A, Baleanu D, Alsaedi A. Analysis of time-fractional Hunter-Saxton equation: a model of neumatic liquid crystal. Open Physics 2016 Jan 1;14(1): 145–9.
[56] Atangana A, Alqahtani RT. Modelling the spread of river blindness disease via the caputo fractional derivative and the beta-derivative. Entropy 2016 Jan 26;18(2): 40.
[57] Ortigueira MD. Comments on "Modeling fractional stochastic systems as non-random fractional dynamics driven Brownian motions". App Math Model 2009 May 1;33(5):2534–7.
[58] Tarasov VE. No violation of the Leibniz rule. No fractional derivative. Communications in Nonlinear Science and Numerical Simulation. 2013 Nov 1;18 (11):2945-8.
[59] Cresson J, Szafrańska A. Comments on various extensions of the Riemann-Liouville fractional derivatives: About the Leibniz and chain rule properties. Commun Nonlinear Sci Numer Simul 2020 Mar;1(82):104903.
[60] Teodoro GS, Machado JT, De Oliveira EC. A review of definitions of fractional derivatives and other operators. J Comput Phys 2019 Jul;1(388):195–208.
[61] Ismael HF, Bulut H, Baskonus HM, Gao W. Dynamical behaviors to the coupled Schrödinger-Boussinesq system with the beta derivative. AIMS Math 2021 Jan 1;6 (7):7909–28.
[62] Kumar D, Paul GC, Seadawy AR, Darvishi MT. A variety of novel closed-form soliton solutions to the family of Boussinesq-like equations with different types. J Ocean Eng Sci 2022 Dec 1;7(6):543–54.
[63] Yepez-Martinez H, Gómez-Aguilar JF. Optical solitons solution of resonance nonlinear Schrödinger type equation with Atangana's-conformable derivative using sub-equation method. Waves Random Complex Media 2021 May 4;31(3): 573–96.
[64] Wang X, Ehsan H, Abbas M, Akram G, Sadaf M, Abdeljawad T. Analytical solitary wave solutions of a time-fractional thin-film ferroelectric material equation involving beta-derivative using modified auxiliary equation method. Results Phys 2023 May;1(48):106411.
[65] Agrawal GP. Fiber-optic communication systems. John Wiley & Sons; 2012 Feb 23.
[66] Ghanbari B, Bekir A, Saeed RK. Oblique optical solutions of mitigating internet bottleneck with quadratic-cubic nonlinearity. Int J Mod Phys B 2019 Aug 10;33 (20):1950224.
[67] Akther S, Hafez MG, Ferdous F. Oblique resonance wave phenomena for nonlinear coupled evolution equations with fractional temporal evolution. Euro Phys J Plus 2019 Sep 1;134(9):473.
[68] Van Gent MR, Van der Werf IM. Influence of oblique wave attack on wave overtopping and forces on rubble mound breakwater crest walls. Coast Eng 2019 Sep;1(151):78–96.